1

2

3

4 **WNT vampirization by glioblastoma leads to tumor growth and**

5 **neurodegeneration**

6 Marta Portela[1*], Varun Venkataramani[2,3,4], Natasha Fahey-Lozano[1], Esther Seco[1],

7 Maria Losada-Perez[1], Frank Winkler[2,3] and Sergio Casas-Tintó[1*]

8 1- Instituto Cajal-CSIC. Av. del Doctor Arce, 37. 28002. Madrid. Spain

9 2- Neurology Clinic and National Center for Tumor Diseases, University Hospital

10 Heidelberg, INF 400, 69120 Heidelberg, Germany

11 3- Clinical Cooperation Unit Neurooncology, German Cancer Consortium (DKTK),

12 German Cancer Research Center (DKFZ), 69120 Heidelberg, Germany

13 4- Institute for Anatomy and Cell Biology, Heidelberg University, 69120 Heidelberg,

14 Germany.

15

16 Corresponding author: scasas@cajal.csic.es and m.portela@cajal.csic.es

17

18

19

20 Running title: Glioma-induced neurodegeneration

21

1

22   **Summary**

23   Glioblastoma (GB) is the most lethal brain tumor due to its high proliferation,

24   aggressiveness, infiltration capacity and resilience to current treatments. Activation of

25   the Wingless-related-integration-site (WNT) pathway is associated with a bad

26   prognosis. Using *Drosophila* and primary xenograft models of human GB, we describe

27   a mechanism that leads to the activation of WNT signaling [Wingless (Wg) in

28   *Drosophila*] in tumor cells. GB cells display a network of tumor microtubes (TMs) which

29   enwraps neurons, accumulates Wg receptor Frizzled1 (Fz1), and, thereby, actively

30   depletes Wg from the neurons. Consequently, GB cells proliferate due to β-catenin

31   activation, and neurons degenerate due to Wg signaling extinction. This novel view

32   explains both neuron-dependent tumor progression, and also the neural decay

33   associated with GB.

34   **Keywords**

35   Neuron, Glia, Cancer, Synapse-loss, wingless, Frizzled, beta-catenin, Glioblastoma,

36   Cytoneme, Wg-depletion.

37

38   **Introduction**

39   The evolution of glioblastoma (referred here as GB) is accompanied by broad

40   neurological dysfunctions, including neurocognitive disturbances, that compromise

41   quality of life during the short life span of patients, one year usually [1]. These tumors are

42   often resistant to standard treatments which include resection, radiotherapy and

43   chemotherapy with temozolomide [2]. Numerous studies are focused on new molecular

44   targets to treat GBs [3-6] ; however, none of them has proven effective yet, which is in

45   stark contrast to the considerable progress made in other tumor types. It is therefore

46   necessary to explore new biological concepts that can lead to additional therapeutic

47   strategies against GBs.

48   The WNT canonical pathway is activated upon the ligand "Wingless-related integration

49   site" (WNT) binding to specific receptors (LRPs and FZD) in the plasma membrane. As

50   a consequence, the destruction complex (APC and Axin) is inactivated and β-catenin

51   (armadillo in *Drosophila*) is released. Further, β-catenin translocates into the cell

52   nucleus where it promotes the expression of target genes (*i.e. Cyclin D1* and *Myc*) [7-8].

53   The WNT pathway is conserved through metazoans and it plays a central role in brain

54   development [9], adult neuronal physiology [10] and synaptogenesis [11]. Perturbations in

55   WNT signaling are associated with neural deficits, Alzheimer´s disease and brain

56   cancer, most notably GB [12]. WNT and FZD signaling can be deregulated in

57   glioblastoma [13-14] (reviewed in [15]). In particular, one of the hallmarks of bad prognosis is

58   the accumulation of ß-catenin in tumoral cells [16-17], indicating an activation of WNT/FZD

59   pathway [18].

60   GB cells extend ultra-long membrane protrusions that interconnect tumor cells [19].

61   These tumor microtubes (TMs) are associated with the worst prognosis in molecular

62   subtypes of human gliomas. TMs contribute to invasion and proliferation, resulting in

63   effective brain colonization by GB cells. Moreover, TMs constitute a multicellular

64   network that connects GB cells over long distances, a feature that likely provides

65   resistance against radiotherapy, chemotherapy and surgery [19-20]. Considering the many

66   cytological similarities of TMs and tunneling nanotubes (TNTs) [21], it seems that TMs in

67   aggressive gliomas are the in vivo correlate of TNTs described in cell culture. In

68   addition, TMs seem akin to a basic mechanism of cell-cell connection and molecular

69   communication called "cytonemes" in *Drosophila* [22]. *Growth Associated Protein-43*

70   (*GAP43*) is essential for the development of TMs and, thus, the tumor cell network

71   which is associated with GB progression [19]. However, many aspects of this

72   paradigmatic finding in glioma biology are still unexplored, including its impact on

73   neighboring neurons.

74   Here, we report that *Drosophila* glial cells develop a TM network upon oncogenic

75   transformation, akin to what is known from refined mouse glioma models, and from

76   patients [19]. These TMs share characteristics in common with *Drosophila* epithelial

77   cytonemes [22-23] which are also dependent on igl/*Gap43* expression. TMs relocate

78   Frizzled (Fz1) receptor in the glia-neuron interphase, depleting Wingless (Wg) from

79   neighboring neurons. As a consequence, the number of glioma cells increases, while

80   neuronal synapse number decreases and neurodegeneration ensues. The concept of a

81   Wg/Fz1 signaling equilibrium between glioma cells and neurons is relevant because it

82   redefines GB as a neurodegenerative disease, and because it reveals a potential novel

83   strategy against GB.

84

85   **Results**

86   ***Drosophila* glioma network**

87   To study the mechanisms of communication among malignant glial cells and

88   neighboring neurons, we used a previously described *Drosophila* GB model [24], which

89   consists in the co-overexpression of constitutively active forms of EGFR (dEGFRλ) and

90   the PI3K catalytic subunit p110α (PI3K92E) driven by the glial specific *repo-Gal4.* This

91   combination stimulates malignant transformation of post-embryonic larval glia, leading

92   to lethal glial neoplasia [24-25] which is measured by the increase of glial cell number

93   (GFP^{NLS} positive) compared with a control brain (Figure 1A-C). Based on

94   this *Drosophila* GB model we have evaluated the impact of glial tumor cell proliferation

95   on neighboring neurons.

96   To visualize the total volume of the glial plasma membrane in larval brains, we

97   expressed a myristoylated form of red fluorescent protein (expressed via *UAS-*

98   *myrRFP*). RFP signal in control brains shows glial soma and the network formed

99   among WT glial cells (Figure 1D, D´). Relative to the control brain, the glioma brain

100   shows a significant enlargement in glial membrane volume (Figure 1E, E´).

101   In addition, we obtained transmission electron microscopy (TEM) images to visualize

102   glia morphology in control samples (Figure 1F-H). High magnification TEM images

103   show an enlargement of glial cells surface in glioma brain samples (Figure 1I), and the

104   infiltration of glioma cells projections through the brain (Figure 1J). Glioblastoma tumor

105   microtubes (TMs) are described in human GB samples as a cell to cell communication

106   system [19], we describe here comparable structures in *Drosophila* glioma brain samples.

107   Magnifications of TEM images show the detail of perineuronal nests of TMs which

108   surround and isolate neurons (Figure 1K-L).

109

110   TMs share characteristics with the cytonemes previously described in epithelial

111   *Drosophila* cells [19]. Ihog (*interference hedgehog*) is a type 1 membrane protein shown

112   to mediate the response to the active Hedgehog (Hh) protein signal [26], which

113   accumulates in the epithelial cytonemes [27].To visualize glia projections in the entire

114   brain of *Drosophila*, we expressed a *UAS-Ihog-RFP* construct under the control of

115   *repo-Gal4*. This red fluorescent tagged form of Ihog-RFP in epithelial cells labels

116   cellular processes (cytonemes) in the basal region of the wing imaginal discs [27-28]. The

117   expression of *UAS-Ihog-RFP* under the control of *repo-Gal4* allows the visualization of

118   projections in wild type glial that build an interconnecting network (Figure 1M, M´). The

119   accumulation of Ihog in the cellular projections of transformed glial cells allowed

120   labeling of the TMs-like processes (Figure 1N, N´). We used 3D reconstructions

121   (IMARIS Bitplane, see materials and methods) from confocal stacks of images to

122   quantify the volume of glial membrane projections, and we observed an expansion of

123   TMs in glioma as compared to control brains (Figure 1O). Since the term tumor

124   microtubes (TMs) is the now established terminology to describe thin membrane

125   protrusions from malignant glioma cells in human and murine tumors [19], we decided to

5

126   also use this term from here on for membrane protrusions in GB *Drosophila* cells

127   observed across the brain.

128   To determine if TMs expand as a consequence of the increase in the number of GB

129   cells, we quantified the volume of the TMs and divided by the number of glial cells

130   (Figure 1P). The results show that TMs volume/glial cell number ratio is higher in GB

131   and therefore we conclude that TMs grow in GB.

132   A detailed analysis of the contact region between neuron and GB cells revealed that

133   glial TMs wrap clusters of neurons in individual GB "nests" (Figure 1K, L compared with

134   G, and see video S1 and S2), this organization is comparable to previously described

135   perineuronal nests in GB patients [29]. To confirm the neuronal identity of the cells within

136   the nests, we used antibodies to specifically mark neurons (anti-Hrp and anti-ELAV,

137   green in Figure 1Q-R) and the Ihog-RFP or myr-RFP to visualize the TMs. The results

138   show that TMs infiltrate within neuronal groups and enwrap neurons which segregate

139   neuronal populations.

140   TMs were previously described to be actin based projections (as cytonemes) [19], to

141   further determine the identity of the TMs in *Drosophila* glioma cells, we took advantage

142   of the LifeActin-GFP reporter and observed in confocal images that TMs (ihog positive)

143   are also actin-based (Figure S1A-C´´´). Moreover, confocal 3D reconstructions

144   (IMARIS, bitplane) of control and glioma brains with the glial network marked with ihog-

145   RFP and LifeAct-GFP showed that actin based TMs form perineuronal nests (Figure

146   S1A-B´´´ and Videos S4-S5). Additionally we characterized the TMs with four

147   previously described markers for cytonemes in *Drosophila* [28] and orthologues markers

148   of human TMs [19,28] (GMA-GFP, GPI-YFP, GFP-MLC and Sqh-GFP in Figure S1D-G).

149   Moreover, we performed functional experiments (Figure S1 H-I´´) where the TMs

150   marked with ihog-RFP, are defective after the downregulation of *neuroglian* (*nrg-RNAi*)

151   as it has been previously described in epithelial cytonemes [30]. All these results together

152   suggests that glioma cells build an organized TMs network around the neurons.

153   Next we sought to clarify whether similar molecular machineries are involved in human

154   and *Drosophila* TMs. Growth-Associated protein 43 (GAP43) is necessary for TMs

155   formation and function, and drives microtube-dependent tumor cell invasion,

156   proliferation, interconnection, and radioresistance [19]. We have reproduced this specific

157   and unique characteristic of human GB in the *Drosophila* model. To determine whether

158   the *Drosophila* glial network is susceptible to *GAP43* depletion, as it has been

159   described in human tumor cells [19], we knocked down *igloo* (*igl*), the invertebrate GAP-

160   43-like gene [31], in glioma cells. Confocal images of larval brains show that the glioma

161   network does not develop upon *igl* silencing and, as a consequence, glial TMs do not

162   enwrap neurons showing a phenotype similar to the control (Figure S1J-L´ and video

163   S1-3).

164   To exclude the possibility that suppression of TMs expansion and glioma progression

165   was due to a titration of GAL4 activity caused by introducing an additional UAS-

166   transgene, we also tested whether co-expression of *UAS-lacZ* or *UAS-yellow-RNAi* had

167   any rescuing ability in glioma brains. The observed phenotypes such as the number of

168   glial cells and the GB nests were unchanged in the presence of an additional UAS-

169   transgene (Figure S2A-B). This observation indicates that in *Drosophila* glioma igl

170   reproduces the function previously described in human samples.

171   The genetic disruption of igl/*Gap43* prevents the tumoral network of TMs and halts the

172   overgrowth of glioma cell membranes. Moreover, the direct consequence on flies

173   developing a glioma is larval/pupal lethality. Upon *igl* knockdown, however, the glioma-

174   induced lethality is prevented allowing the emergence of adults (Figure S1M).

175   Interestingly, *igl* knockdown in wild type glial cells neither affects the normal

176   development of neurons and glia, nor their viability (Figure S2C-G). Taking all data

7

177   together, transformed glial cells take advantage of the igl/Gap43-dependent tumoral

178   network to proliferate and enwrap neurons and, as a consequence, cause death. Thus,

179   the dependency of TMs on igl/GAP43 is conserved between flies and gliomas

180   originated from human tumor cells.

181   **Wingless signaling in glioma**

182   GB is characterized by the deregulation of many key signaling pathways involving

183   growth, proliferation, survival, and apoptosis, such as p53, pRB, EGFR, PI3K, STAT3

184   or WNT [32-33]. WNT signaling has long been suggested as a hallmark in gliomagenesis

185   associated with the proliferation of stem-like cells in human GBs [34]. WNT signaling

186   promotes tumoral cell proliferation and dissemination as well as resistance to chemo

187   and radiotherapy (reviewed in [15,35]). To assess the prevalence of WNT genes/pathway

188   deregulation in GB, we searched for mutations related to WNT pathway in the

189   Collection of Somatic Mutations in Cancer (COSMIC). We analyzed data from 922

190   samples of grade IV astrocytomas (GB) searching for gain of expression or

191   duplications. First, we analyzed *Wnt* family genes, which encode the ligands of the

192   WNT pathway. In particular, we analyzed WNT6 that is related to the self-renewal

193   ability of GB cells [36], WNT3A and WNT1 overexpression that is detected in glial stem

194   cells [37] and WNT5A and WNT2 that were shown to induce migration of GB cells [38-39].

195   Our analysis of the COSMIC database revealed that WNT1, WNT3A, WNT6 or WNT5A

196   genes do not appear mutated in GB samples and only 6 cases showed mutations in

197   WNT2 (0,6%) (Figure S3A). WNT signaling is a hallmark of GBs, but as no evident

198   changes in WNT expression were found, we searched for mutations in FZD genes, that

199   encode the receptors of WNT. In particular, we analyzed FZD2 and FZD9 that are

200   linked to self-renewal ability in GB [36,39-40] and FZD4, a positive WNT regulator, which is

201   a causative effector for invasive phenotypes of GB cells [41]. We did not find any case of

202   a GB patient with a gain of expression in FZD2 or FZD4, and barely 4 cases (0,4%)

203   showed a mutation for FZD9. The total number of mutations related with WNT or FZD

204   genes accounts for 5% of the total GB samples analyzed (Figure S3A). In addition, we

205   analyzed data from GB in The Cancer Genome Atlas (TGAC) for WNT ligands, FZD

206   receptors and transcriptional targets of WNT pathway databases (Figure S3B-D)

207   through the Xena Functional Genomics Explorer (https://xenabrowser.net/). We

208   analyzed expression levels in primary GB tissue and non tumoral tissue, transcriptional

209   targets for WNT pathway (Figure S3B) are upregulated in GB samples. However, WNT

210   ligands from the canonical WNT pathway are not upregulated (Figure S3C) and among

211   FZD receptors, only FZD7 shows significant changes in GB tissue (Figure S3D).

212   Taking all these data together, in spite of WNT pathway activation in GB tissue, there is

213   no correlation between overexpression of WNT ligands and GB development.

214   Nevertheless, previous reports indicate that WNT targets, such as FoxM1 which

215   promotes nuclear localization of β-catenin, or β-catenin itself are related with Glial

216   Stem Cells (GSC) maintenance and tumorigenesis. Indeed, they are standard

217   biomarkers for GB bad prognosis [16,42-45]. β-catenin activation (translocation to the

218   nuclei) is a downstream event of WNT pathway. It has been identified in 19% of

219   surgical samples from adult GB patients and in 30% of surgical samples from pediatric

220   patients. Moreover, WNT inhibition leads to suppression of tumor growth, proliferation

221   in cultures, and a modest induction of cell death [34].

222   Given the discrepancy between the presence of WNT pathway markers and the lack of

223   mutations in GB samples, we decided to study *Wingless* (*wg*) expression, the fly

224   homologue to human WNT, in our glioma model. We quantified anti-Wg signal intensity

225   in glial cells and neuronal tissue and obtained the Wg in glia vs Wg in neurons pixel

226   intensity ratio. The results showed that Wg protein is homogeneously distributed in

227   control larval brains with a slight increase (1,5 ratio) in glial membranes (Figure 2A-A´´,

228   C) but glioma brains showed a four-fold increase in accumulation of Wg in tumoral cells

229   (Figure 2B-B´´, C), in line with WNT accumulation in human GBs [38,46]. To determine

230   whether Wg could be signaling to the glial cells, we assessed the presence of Frizzled

231   (Fz) receptors in glial membranes. Monoclonal antibodies were used to visualize the

232   Fz1 and Fz2 receptors in control samples, the quantification of anti-Fz1 signal in glia vs

233   neurons shows that Fz1 receptors are localized homogeneously across the brain with a

234   small accumulation in glial membranes (Fz1, Figure 2D-D´´, H). Fz2 staining shows the

235   expected pattern in the wing disc [47] as a control (Figure S4A) and it is localized

236   homogeneously in control brains S4B-B´´´). However in glioma samples, Fz1 is highly

237   accumulated in glial membranes (Figure 2E-E´´, H). No changes for Fz2 were detected

238   in glioma brains (Figure S4C-C´´´). In addition, a detailed analysis of glioma brains

239   revealed that Fz1 protein specifically accumulated in TMs (iHog$^+$) (Figure 2E''). The

240   results indicate that Fz1 is preferentially accumulated in perineuronal nests of TMs, in

241   contact with neighboring neurons. These data suggest that the glioma TMs network

242   contributes to Wg/Fz1 signaling.

243   To evaluate the contribution of Fz1 to the progression of the glioma, we knocked down

244   the Fz1 receptor (using *UAS-Fz1-RNAi*) in transformed glial cells. First we validated

245   *UAS-Fz1-RNAi* tool in epithelial tissue from larvae wing imaginal discs. Even though

246   Fz1 expression in wing imaginal disc is discrete, upon *UAS-Fz1-RNAi* expression in the

247   posterior compartment (marked with GFP), there is a reduction in Fz1 protein signal

248   compared with the anterior compartment from the same tissue (Figure S5A). Brains

249   showed a significant reduction of Fz1 protein expression (Figure 2F, H). However, TMs

250   network was still formed (Figure 2F'). Furthermore, we inhibited the development of the

251   glioma network by expressing *UAS-igl-RNAi* and stained the brains for Fz1. Under

252   these conditions the network does not expand, Fz1 does not accumulate in TMs and it

253   shows a homogeneous distribution comparable between glia and neurons (Figure 2G-

254   G´, H). These results indicate that Fz1 accumulation in TMs is a consequence of the

255   glioma network but suggests that Fz1 accumulation in the TMs is dispensable for

256   glioma network formation.

257   **Glial Fz1 interacts with neuronal Wg**

10

258   The abnormal distribution of Wg and Fz1 in glioma brains could be due to either an

259   increase in gene expression or to redistribution of the protein. First, to determine *wg*

260   and *Fz1* transcription levels in glioma, we performed quantitative PCR experiments

261   from brain RNA extracts. The results showed that *wg* and *Fz1* transcription levels are

262   comparable in control and gliomas (supp. Figure S6A). To consider the mRNA

263   translation or protein stability and degradation, we measured total Fz1 and Fz2 protein

264   levels in Western blot experiments. Control and glioma brain protein extracts were

265   blotted and incubated with anti-Fz1 or Fz2 antibodies; Tubulin was used as a loading

266   control (Supp. Figure S6B). Quantification of the membranes showed no significant

267   changes for Fz1 protein levels in glioma (Supp. Figure S6B). Moreover, we performed

268   *in situ* hybridization experiments to detect Wg and Fz1 mRNA expression in control and

269   glioma brains. The results are consistent with the qPCRs results (Figure S6A) showing

270   no differences for *wg* or *Fz1* transcription between controls and gliomas (Figure S6C).

271   The data indicate that in spite of a higher signal for Wg and Fz1 proteins in glioma cells

272   by immunofluorescence, there are no changes in gene expression. We hypothesized

273   that Fz1 is transported and accumulated along glioma TMs, which contact neighboring

274   neurons and receive Wg from them.

275   According to this hypothesis, the glial membranes would be in close proximity to

276   neuronal membranes to allow Fz1-Wg interaction. To assess this, we performed

277   GRASP experiments [48]. This technique determines intimate physical interaction among

278   glia and neurons, in the range of 20-40nm (synaptic distance) which is compatible with

279   protein-protein interaction [48]. Each split fragment of the green fluorescent protein (GFP)

280   was expressed in neurons (*elav-lexA*) or glial (*repo-Gal4*) cells, respectively (see

281   Material and Methods). Only upon intimate contact between the two split fragments

282   GFP fluorescence is reconstituted. Control samples (Figure 3A-C´´) showed a discrete

283   signal corresponding to the physiological interaction between glia and neurons,

284   nevertheless, upon glioma induction a massive GFP signal from GRASP reporter was

11

285 detected (Figure 3D-F´´). This result indicates that, in a glioma condition, there is a

286 significant increase of glia-neuron membrane interaction, consistent with the TEM

287 images (Figure 1H-L) showing perineuronal nests of TMs which surround and isolate

288 neurons.

289 We had observed specific signal localization for Wg and Fz1 in glioma membranes

290 (myr-RFP/ihog-RFP) (Figure 2B-B´´, E-E´´). To confirm the physical interaction of Fz1

291 and Wg proteins we performed proximity ligation assays (PLA) (see Materials and

292 Methods) [49]. This quantitative method reports the interactions between two proteins

293 with a resolution of 40nm [50]. Control brains showed a discrete number of puncta

294 showing the physiological interactions (Figure 3G-H´ and quantifications in 3I, J)).

295 However, glioma brains showed a five-fold increase in the number of PLA$^+$ puncta

296 (Figure 3H´,I, J) indicating a significant increase in the number of Fz1-Wg interactions.

297 Moreover, we calculated the number of Wg-Fz1 interactions per glial cell in control and

298 glioma brains and the results show that the number if interactions per cells is higher in

299 the glioma brains (Figure 3J). These results confirm that glioma cells accumulate Fz1

300 receptor in TMs, and then this specific receptor interacts with Wg. But Wg is not

301 upregulated in the glioma brain so we hypothesize that Wg comes from neighboring

302 neuronal membranes and it relocates and accumulates in glioma cell membranes.

303 **Wg/Fz1 pathway targets are active in glioma and inactive in neurons**

304 Wg targets are indicators of Wg/Fz1 activity in the recipient cell. Armadillo/βCatenin is

305 a cytoplasmic protein which, upon activation of Wg pathway, translocates into the

306 nucleus and activates transcription of target genes [12,51]. To determine if Fz1 is signaling

307 in gliomas as a consequence of Wg-Fz1 interaction, we stained control and glioma

308 brains for Armadillo (Arm) with a specific antibody that detects Arm protein and is

309 mainly visible in its cytoplasmic inactive form (Cyt-Arm) [52]. Cyt-Arm was

310 homogeneously distributed along the brain in control samples (Figure 4A, D). However,

311   glioma brains showed accumulation of Cyt-Arm in the cytoplasm of the neurons and a

312   reduction in glioma cells (Figure 4B, D). This result suggests that, in glioma brains,

313   Wg/Fz1 pathway is inactive in neurons and active in glioma cells. More importantly, this

314   data shows that the network expansion and the accumulation of Fz1 in the TM

315   projections have an effect on neighboring neurons. Further, we dismantled the glioma

316   network expressing *UAS-igl-RNAi* or downregulated Fz1 (*UAS-Fz1-RNAi*) and stained

317   for Cyt-Arm. Under this condition, Cyt-Arm was homogeneously distributed along the

318   brain similar to the control (Figure 4C, D and S7A) demonstrating that the network is

319   required to promote Wg signaling in the transformed glia.

320   To further confirm that Wg pathway is active in the glial transformed cells and silenced

321   in neurons, we used five additional Wg pathway reporters, namely *arm-GFP, nkd-lacZ,*

322   *tsh-lacZ, fz4-GFP* and *dally-LacZ* [54-55]. The results showed that all these reporters were

323   active in glioma cells and inactive in neurons compared to control brains (Figure4E-H

324   and Figure S7B-G´´) which confirm that the Wg/Fz1 pathway is inactive in neurons

325   confronted to a GB, and active in GB cells.

326   Since we observed specific signal localization and accumulation of Wg and Fz1 in

327   glioma membranes and consequently the activation of the pathway in glioma cells, we

328   wondered if these results were conserved in human glioma cells. Therefore, we used a

329   primary patient-derived glioblastoma culture xenograft model using S24 cells kept

330   under stem-like conditions (see Materials and Methods), which reproduce previously

331   described Scherer modes, perivascular migration and spread [29,56]. GFP-marked S24

332   cells were injected in the brain of NMRI nude mice, and brains were removed and

333   analyzed 90 days later (as previously described in [19]). To validate our data, we

334   performed a series of more diffuse tumor parts (history grade II-like tumor periphery

335   where normal brain has just been colonized) and denser tumor parts (grade III-IV like,

336   from central areas) GB images from S24 xenografts brain sections.

337   We stained the samples for β-catenin and WNT1 proteins in S24 xenograft brain

338   sections and compared them to control samples (Figure 4I-N and Figure S8G-H). We

339   observed a significant increase of both proteins in GB cells, in line with previous

340   observations. These data indicate that WNT1 is deposited in GB cells and activates

341   WNT pathway; consequently β-Catenin is upregulated to mediate GB cells malignancy

342   [16]. Moreover, images of the WNT1 and βCatenin staining of grade II and III GB images

343   from S24 xenografts brain sections and quantification of the pixel intensity indicates

344   that the accumulation of WNT1 and activation of βCatenin correlates with the growth of

345   the tumor (Figure S8A-F).

346   To determine Fz1's contribution to the proliferation of *Drosophila* gliomas we quantified

347   the number of transformed glial cells upon *Fz1* downregulation. A specific Repo

348   antibody was used to mark glial cell nuclei in the brains. The data show a significant

349   increase of glial cell number in glioma brains, which is prevented by *Fz1*

350   downregulation or TM network dismantlement (Figure 5A-E). In addition, we studied

351   the adult survival by quantifying the number of flies with glioma and/or *Fz1-RNAi*

352   expression. First, Fz1 downregulation in normal glial cells allows 80% adult survival.

353   On the other hand, the glioma caused 100% lethality in larval or pupal stages. By

354   contrast, glioma lethality was reverted upon *Fz1* downregulation in repo cells, and 70%

355   of the animals reached adulthood (Figure 5F). In conclusion, Fz1 is not necessary for

356   the glioma network overgrowth but Wg/Fz1 signaling is necessary for the increase in

357   the number of tumoral cells and the associated lethality.

358

359   **Wg/Fz1 pathway disruption in adult brains**

360   To discard that these results are restricted to a developmental process, we performed

361   similar experiments in adult brains. We included the *tub>Gal80^{TS}* system to repress

362   Gal4 activation during all developmental stages (see Materials and Methods), glioma

363   was induced 4 days after adult eclosion when adult brain is fully differentiated. Analysis

364   of adult flies survival indicate that animals with glioma start dying at day 9 after the

365   glioma induction until the 14th day, significantly earlier that control flies. (Figure S9A). 7

366   days after glioma induction we stained for Cyt-Arm, Fz1 and Wg control and glioma

367   adult brain samples and quantified (n>15) the average pixel intensity ratio (Glial cells

368   membranes RFP+ vs neuronal tissue (Figure S9B-H). The results reproduce the

369   findings from larval brains: Fz1 and Wg proteins are accumulated in glioma tissue and

370   Cyt-Arm signal shows an increase of wg-pathway activity in glioma cells. Therefore,

371   there are no differences between larval and adult brains regarding Wg-pathway in

372   glioma cells and neurons. Moreover, we analyzed *Drosophila* adult negative geotaxis

373   behavior (climbing assay), as an indication for possible motor defects associated with

374   neurodegeneration. The results showed symptoms of neurodegeneration in glioma flies

375   compared to controls (Video S6).

376   **Gliomas cause Neurodegeneration**

377   Previous results suggest that a neurodegeneration process is taking place in glioma

378   brains. To determine whether the glioma is causing neurodegeneration we quantified

379   the number of active zones (synapses) in the neuromuscular junction (NMJ). This well-

380   established system has been used for decades to study neurodegeneration in

381   *Drosophila* [57-60], motor neuron soma is located in the central nervous system, but

382   synapse counting can be accurately done in synaptic buttons located in adult or larva

383   muscular wall. Adult NMJs Quantification of confocal images stained with anti-

384   bruchpilot (Nc82) revealed a significant reduction in the number of synapses in glioma

385   adult (Figure S9I) or larval NMJs compared to controls (Figure 6A-B, F) and therefore,

386   a neurodegenerative process, which is prevented by Fz1 downregulation or TM

387   network dismantlement (igl downregulation) (Figure 6C-D, F).

388

389   **Wg expression in glioma cells is dispensable for tumor progression**

390   Fz1 receptor is accumulated in glioma TMs and contributes to Wg depletion and

391   pathway equilibrium disruption. To determine whether the source of Wg is neuronal or

392   glial, we silenced *wg* expression in neurons exposed to glioma, or in glioma cells. First

393   we validated *UAS-wg-RNAi* tool in epithelial tissue, wing imaginal discs. Activation of

394   *UAS-wg-RNAi* in the posterior compartment (marked with GFP) cause a reduction of

395   specific monoclonal anti-wg (Figure S5B). Pan-neuronal *wg* silencing (*elav>wg RNAi*)

396   is lethal in line with our hypothesis regarding the requirement of Wg in neuronal

397   biology. Besides, *wg* knockdown (*wg-RNAi*) in glioma cells (*Repo>PI3K; EGFR; wg-*

398   *RNAi)* does not prevent glioma cell number increase (Figure 6G-I, K) nor glioma TMs

399   volume expansion (Figure 6G-I, L), these results suggest that *wg* expression in glioma

400   cells is not relevant for glioma progression.

401   Moreover, to stress on the contribution of Fz1 receptor as mediator for Wg depletion,

402   we generated glioma cells and silenced *Fz1* expression, in addition we expressed a

403   constitutively active form of *armadillo* (*UAS-armS10*) [61] to activate Wg pathway

404   downstream Wg-Fz1 in these gliomas (Figure 6E-F and J-L). We counted the number

405   of synapses and observed that it is comparable to glioma + *Fz1RNAi* (Figure 6C-F).

406   This result suggests that the reduction in the number of synapses is specifically

407   mediated by Fz1 accumulation. To confirm that the Fz1 depletion and Arm signaling

408   produces a glioma like condition we counted the number of glial cells and TM network

409   volume (Figure 6G-L). We observed that in this case the number of glioma cells

410   increased and TMs expanded (Figure 6J-L) similar to a glioma (Figure 6H).

411   **Wg/Fz1 pathway disruption causes neurodegeneration**

412   Neuronal development and physiology are dependent on Wg/Fz1 signaling and

413   disruptions in this signaling pathway lead to synapse loss, an early symptom of

414   neurodegeneration (reviewed in [62-65]. To determine if an imbalance in Wg distribution

16

415   caused by glioma cells can affect the neighboring neurons, we aimed to determine the

416   contribution of Fz1/Wg pathway to neuronal physiology. To inhibit Wg/Fz1 pathway

417   signaling we expressed *UAS-fz1-RNAi* or *UAS-wg-RNAi* in motor neurons under the

418   control of a *D42-Gal4* driver [66] and quantified the number of active zones (synapses) in

419   the neuromuscular junction (NMJ). Quantification of confocal images stained with anti-

420   bruchpilot (Nc82) revealed a significant reduction in the number of synapses and

421   therefore, a neurodegenerative process (Figure 7A-D). These data suggest that

422   Wg/Fz1 signaling pathway activity in neurons is necessary in for synaptogenesis.

423   So far, we have demonstrated that glioma cells cause a disruption of Wg/Fz1 signaling

424   in neurons (Figure 4) and our data suggest that this is dependent on Fz1 accumulation

425   in glioma cells (Figure 2). Next, we decided to restore this signaling equilibrium by

426   overexpressing Fz1 receptor in neurons surrounded by glioma cells. To avoid crossed

427   expression we generated Fz1 transgenic flies based on the LexA-LexAop expression

428   system [67] , which is independent of the Gal4-UAS system used to generate the glioma.

429   We validated this newly generated tool in *Drosophila* brains. *LexAop-Fz1* was activated

430   in neurons under the control of *elav-LexA* and monoclonal anti-Fz1 showed higher

431   signal in neurons and functional activity revealed by anti-Arm staining (Figure S5C-E).

432   Oversized glioma brains showed the expected glioma network compartmentalizing

433   neurons in the brain (Figure 7E-F´´). However, Fz1 overexpression in neurons restored

434   homogeneous Fz1 protein distribution in the brain (Figure 7G, H), rescued brain size

435   (Figure 7G-G´´) and neuron distribution and morphology (Figure 7H´-H´´). In addition,

436   Fz1 equilibrium restoration partially rescued lethality and most animals reached

437   adulthood. To verify Fz1 activation of the pathway we stained for Wg and Cyt-Arm

438   (Figure S10). As previously shown, glioma brains showed a heterogeneous distribution

439   for Wg protein (Figure S10A-A´´) and, as a consequence, an imbalance in pathway

440   activation reported by Cyt-Arm accumulation (Figure S10 C-C´´). As expected,

17

441   neuronal Fz1 overexpression in glioma brains restored Wg distribution and Cyt-Arm

442   signal to a control situation (Figure S10B-B´´, D-D´´)

443   To further determine the effect of Wg/Fz1 signal restoration in neurons, we quantified

444   the number synapses in their NMJs. Neuronal morphology is disrupted by glioma

445   (Figure 7I, J) and restored by Fz1 overexpression in neurons neighboring glioma cells

446   (Figure 7J, K). Moreover, synapse number reduction upon glioma induction is restored

447   by Fz1 overexpression in neurons (Figure 7L). All these results indicate that the

448   Wg/Fz1 pathway disruption caused by glioma is responsible of the synapse loss.

449   Restoration of the signaling equilibrium between glia and neurons prevents synapse

450   loss and therefore, neurodegeneration.

451   **Glioma depletes Wg from neuronal membranes**

452   The actual mechanisms of Wingless delivery have been under debate. This protein

453   was initially described as a diffusible secreted protein [68]. Recent studies have proved

454   that Wg secretion is not necessary for *Drosophila* development [69]. A membrane-

455   tethered version of Wg protein [70] (Wg^{NRT}) can substitute the endogenous gene, mimic

456   Wg normal functions and produce viable organisms [69]. We took advantage of this tool

457   to determine the cellular mechanisms mediating glioma Wg retrieval from neurons. We

458   created a genetic combination to substitute one copy of endogenous Wg with one copy

459   of wg^{NRT} exclusively in neurons (by using the LexAop system). In addition, upon LexA

460   system activation, neurons are marked with membranous GFP (CD8-GFP) while the

461   rest of the cells are wild type. Moreover, this Wg^{NRT} is tagged with an HA which allows

462   to discriminate from the endogenous Wg protein. We induced a glioma and marked the

463   glial cells in red (ihog-RFP) (see materials and methods and Figure 8G). First, we

464   studied normal control brains that express Wg^{NRT} exclusively in neurons in the absence

465   of glioma. We stained with anti-HA and observed a positive signal both in neurons and

466   glial cells but not in the control without the elav-LexA driver, indicating that the HA

18

467   signal is not a false positive (Figure 8A-B, H). Finally, we performed the experiment in

468   the glioma model to examine the interaction of glioma cells with Wg^{NRT} expressing

469   neurons (Figure 8E-F-I) and stained with anti-HA. The images show a homogeneous

470   signal for HA throughout the brain in glia and in neurons (See figure H-I magnifications

471   for more detail), suggesting that glioma cells can deplete this non-

472   secretable/membrane tethered version of Wg from neurons. We have quantified the

473   number of HA^{+} puncta in glia and neuron from control and glioma samples. The results

474   suggest that glial cells are able to sequester membrane anchored Wg^{NRT} from neuronal

475   membranes at comparable rates under both physiological and glioma conditions

476   (Figure 8J). However, there was a detectable reduction in the number of glioma cells,

477   similar to previous results when Wg/Fz1 equilibrium in glial vs neurons was restored

478   (Figure 7C, E and Figure 7G-H´´). Since Wg^{NRT} is anchored to neuronal membranes, it

479   would be expected to reduce the total Wg signaling in glioma cells thereby decreasing

480   cell proliferation/survival, thus resulting in a rather normal sized brain (Figure 8A, C, E).

481   Moreover, heterozygous wg^{NRT}/wg prevented glioma network progression (Figure

482   8D´vs F´). In conclusion, glioma cells produce a network TMs that reach neighboring

483   neurons, increasing intimate membrane contact that facilitates neuronal-Wg

484   sequestering mediated by the Fz1 receptor in glioma TMs. Since Wg/Fz1 signaling in

485   glioma mediates cell number and tumor progression, targeting this cellular interaction

486   may be a new candidate for future therapies.

487

488   **Discussion**

489   In addition to cell autonomous features of tumor cells, including founder mutations,

490   recent evidences indicate that microenvironment signals contribute to glioma

491   progression. Neuroligin-3 (NLGN3) is a synaptic protein cleaved and secreted after

492   neuronal activity which promotes PI3K-mTOR signaling stimulating glioma growth.

493 Thus, NLGN3 mediates an autocrine/paracrine loop in glioma cells which perpetuates

494 tumoral features [71] (reviewed in [72]). Also, neural precursor cells (NPC) from the

495 subventricular zone (SVZ) produce chemoattractants (SPARC/SPARCL1, HSP90B and

496 pleiotrophin) which facilitate glioma invasion of the SVZ through Rho/ROCK signaling

497 [73].

498 We showed recently that TM network formation determines GB tumor malignancy,

499 confers radiotherapy resistance and influences patient's prognosis [19]. TMs stability in

500 GB is sensitive to *GAP43* expression in tumoral cells [19]. Also, *Tweety homologue-1*

501 (*TTHY1*) expression in GB cells, mediated by NLGN3 regulates TM formation [74].

502 This study shows that TMs intercalate among neurons and enwrap them in

503 perineuronal nests [29] structures establishing an intimate link glioma-neuron. Then GB

504 cells make direct contact via TMs and deprive neurons of WNT.

505 Expression data from human cancer databases indicate that glioma cells do not

506 upregulate *Wnt* expression, neither upregulate its receptors, however downstream

507 targets of the pathway such as β-catenin are upregulated. Instead, the results in the fly

508 model show that glioma cells relocate Fz1 receptor in the TMs allowing depleting Wg

509 from neurons. Thus we use the term vampirization as the action of GB cells to exhaust

510 or prey upon healthy cells (neurons) in the manner of a vampire, as they drain

511 Wg/WNT and cause the demise of the neurons. Consistent with these data, in the

512 patient-derived GB xenograft model, where WNT1 is deposited in GB cells and the

513 WNT pathway is activated, β-catenin is upregulated. The available data suggest that

514 GB TMs grow towards the source of Wg. However, as TMs expand upon Fz1/Wg

515 signaling, the question regarding the exact order of events remains open. Do TMs

516 require some initial stimuli from the source of Wg to grow? Alternatively, do TMs initiate

517 growth triggered by glial internal signals and directed through a gradient of neuron-

518 secreted attractants?

519

520 Concerning the mechanism of Wg vampirization, we have expressed a non secretable,

521 HA- tagged version of membrane- tethered Wg[NRT] in neurons. In that experiment Wg is

522 detected within glial cells demonstrating that GB cells can take Wg directly from the

523 neuronal membrane. However, further studies are still required to determine the

524 precise mechanism of neuronal Wg depletion by GB cells TMs.

525

526 It is widely observed that brain tumors and related ailments can cause cognitive decline

527 and neuronal dysfunction (reviewed in [75]). High-grade glioma patients continue to

528 display cognitive deficits after surgery, radiotherapy or chemotherapy [76-78]. The most

529 common deficits concern memory, executive functions and general attention beyond

530 the effects of age, education and gender [79]. Nevertheless, the molecules mediating

531 neuronal degeneration need to be determined.

532

533 Synapse loss is an early step in neurodegeneration [80-82] which is consistent with the

534 cognitive defects observed in GB patients. Nonetheless, cognitive defects can be

535 observed also in patients with excess of synapses as in the case of fragile X syndrome

536 [83-84]. GB cells can stimulate aberrant synapses associated with seizures [85] which are

537 compatible with cognitive dysfunctions. Neuronal death is a later event in

538 neurodegenerative processes such as Alzheimers´s disease [86-88]. In GB patients,

539 neuronal death is under debate and this issue should be addressed with further data.

540 There is preclinical work [88-89] supporting Glioma-induced neuronal death due to

541 glutamate cytotoxicity, in addition clinical studies from [90] support neuronal death in GB

542 patients. However, it is certainly very difficult to draw clear conclusions from clinical

543 samples or clinical courses, considering that therapy, antiepileptics and the pure space

544 occupation plus the edema contribute to the neuronal dysfunction, degeneration and

545 cell death.

546

547   In particular, neuronal cell loss is typically found at and around glioblastomas, and

548   neurocognitive disturbances are a frequent finding in glioma patients. Although

549   evidences from our experience and from neuropathology expertise, this is an open

550   debate which requires further attention.

551

552   The data also reveal that reestablishing Wg signaling equilibrium by Fz1

553   overexpression in neurons, not only restores synapse number but also blocks GB

554   progression. Functional disruption of the equilibrium between GB glia and neurons is

555   described here for the first time. Possibly, this mechanism could be valid for other

556   molecules related to tumor progression such as Notch, Hedgehog or TGF. Moreover,

557   cytoneme-like structures play a role in development and in other cell types [91-93]. Hence,

558   we propose that cytoneme-like structures in physiological conditions and TMs in

559   pathological GB conditions could redistribute limited amounts of signaling molecules

560   among competing cell types, therefore long range redistribution of signaling molecules

561   could be a general mechanism for the cells to compete for different resources.

562

563   This study integrates for the first time the oncogenic nature of glioma with the neuronal

564   degeneration caused by Wg depletion. This innovative concept of glioma-induced

565   neurodegeneration opens the possibility of combined treatments to fight GB

566   progression and associated neurodegeneration at the same time. Our data

567   demonstrate that making the neurons more competitive for secretable factors such as

568   Wg already has an impact in GB tumor growth, although it remains to be demonstrated

569   what type of drugs can carry out these actions.

570

571   The rapid transformation of GB cells and the heterogeneity of mutations in these

572   tumors are a handicap for genetic therapies and monoclonal therapies. In our view,

573   cellular features such as the network shared by GB cells emerge as an alternative to

574   tackle tumor progression. Among the possible new strategies, TMs dynamic and

575 cellular transport of receptors to the TMs could be a target to prevent GB proliferation

576 and neurodegeneration. GAP43 has emerged as a functional component of GB

577 network formation. Recent studies indicate that other proteins such as Flotilin [28,94],

578 participate in cytoneme dynamics. The discovery of molecules regulating TM/cytoneme

579 biology arises as potential targets for cancer treatment.

580

581

582 **Author contributions**

583 Conceptualization, S.C.T. M.P. and FW; Methodology, S.C.T., VR, M.P., M.L.P., E.S.

584 and N.F.; Investigation, S.C.T., FW, VR, M.P. M.L.P, E.S and N.F.; Writing – Original

585 Draft, M.P, FW and SCT.; Writing – Review & Editing, S.C.T. and M.P.; Funding

586 Acquisition, S.C.T and FW.; Supervision, S.C.T.

587

588 **Acknowledgements**

602   Authors declare no conflicts of interest.

603

604 **Experimental Procedures**

605 **Fly stocks**

606 Flies were raised in standard fly food at 25ºC.

607 Fly stocks from the Bloomington stock Centre: *UAS-GFP^{nls}* (BL4776)*, UAS-lacZ*

608 (BL8529)*, UAS-myr-RFP* (BL7119), *UAS-igl-RNAi* (BL29598)*, arm-GFP* (BL8555)*,*

609 *nkd04869a-lacZ* (BL25111)*, D42-Gal4* (BL8816), *GFP-fz1-GFP* (BL59780), *repo-Gal4*

610 (BL7415)*, puc-lacZ, UAS-CD8-GFP* (BL32186)*, tub-gal80^{ts}* (BL7019), *elav-lexA*

611 *(BL52676), lexAop-CD8-GFP* (BL32205), *lexAop-flp* (BL-55819), *UAS-armS10*

612 *(BL4782), sqh-GFP (BL57145), UAS-CD4-spGFP1-10, lexAop-CD4-spGFP11*

613 (obtained from BL58755), *en-Gal4, UAS-GFP (from BL25752)*. Fly stocks from the

614 Vienna *Drosophila* Resource Centre: *UAS-fz1-RNAi* (v105493), *fz4-GFP* (v318152),

615 UAS-*wg-RNAi* (v104579), UAS-*yellow-RNAi* (v106068), *UAS-nrg-RNAi* (v107991)*.*

616 *GFP-sls (MLC, ZCL2144 from http://flytrap.med.yale.edu), UAS-dEGFR^{λ}, UAS-*

617 *PI3K92E* (dp110^{CAAX}) (A gift from R. Read), *UAS-ihog-RFP* (a gift from I. Guerrero)*, tsh-*

618 *lacZ* and *dally-lacZ* (gifts from M. Milan), *lexAop*-fz1 (generated in this study)*, FRT Wg*

619 *FRT NRT–Wg-HA, pax –Cherry (a gift from A. Baena-López)*, *lifeactin-GFP* (a gift from

620 I. Guerrero), for electron microscopy studies, we used the *UAS-HRP:CD2* as reporter

621 [95], *UAS-GPI-YFP* [96], *UAS-GMA-GFP* [97].

622 ***Drosophila* glioblastoma model**

623 The most frequent genetic lesions in human gliomas include mutation or amplification

624 of the Epidermal Growth Factor Receptor (EGFR) gene. Glioma-associated EGFR

625 mutant forms show constitutive kinase activity that chronically stimulates Ras signaling

626 to drive cell proliferation and migration [98-99]. Other common genetic lesions include loss

627 of the lipid phosphatase PTEN, which antagonizes the phosphatidylinositol-3 kinase

628 (PI3K) signaling pathway, and mutations that activate PI3KCA, which encodes the

629 p110a catalytic subunit of PI3K [98-99]. Gliomas often show constitutively active Akt, a

630 major PI3K effector. However, EGFR-Ras or PI3K mutations alone are not sufficient to

631 transform glial cells. Instead, multiple mutations that coactivate EGFR-Ras and

632 PI3K/Akt pathways are required to induce a glioma [29]. In Drosophila, a combination of

633 EGFR and PI3K mutations effectively causes a glioma-like condition that shows

634 features of human gliomas including glia expansion, brain invasion, neuron

635 dysfunction, synapse loss and neurodegeneration [24,100-101]. Moreover, this model has

636 proved to be useful in finding new kinase activities relevant to glioma progression.[25] To

637 generate a glioma in *Drosophila* melanogaster adult flies, we used the Gal4/UAS

638 system [102] as described above (*repo*-Gal4>UAS-*EGFRλ*,UAS-*dp110*. To restrict the

639 expression of this genetic combination to the adulthood, we used the thermo sensitive

640 repression system Gal80^{TS}. Individuals maintained at 17ºC did not activate the

641 expression of the UAS constructs, but when flies were switched to 29ºC, the protein

642 Gal80^{TS} changed conformation and was not longer able to bind to Gal4 to prevent its

643 interaction with UAS sequences, and the expression system was activated.

644 **Generation of Transgenic flies**

645 *LexAop-Frizzled1* construct was generated by RECOMBINA S.L. Fz1 (*CG17697*) CDS

646 was synthesized by overlapping g-block assembly. The complete 17665bp fragment

647 was amplified using the high fidelity Phusion taq polymerase (Thermo fisher Scientific)

648 and *Eco.Friz.Fw* and *Xba.Friz.Rv* primers. PCR amplicon was cloned in pJET entry

649 vector (Thermo Fisher Scientific), then Frizzled fragment was released with *EcoRI*/*XbaI*

650 restriction enzymes and sub-cloned into destination *pLOTattB* plasmid.

651 *Eco.Fz1.Fw* 5´-GAATTGGGAATTCATGTGGCGTCAAATCCTG-3´

652 *Xba.Fz1.Rv* 5´-TCTAGACTAGACGTACGCCTGCGCCC-3´

653 Transgenic flies were injected and *Frizzled1* fragment was inserted in the chromosome

654 2L by the *Drosophila* microinjection service (CBMSO-CSIC) using the following stock:

655 *y[1] M{vas-int.Dm}ZH-2A w[*]; M{3xP3-RFP.attP'}ZH-22A* (BL24481). Transgenic flies

656 were selected individually by eye color (w+) and balanced with *CyO*.

657

Antibodies for Immunofluorescence

658

659   Third-instar larval brains, were dissected in phosphate-buffered saline (PBS), fixed in

660   4% formaldehyde for 30min, washed in PBS + 0.1 or 0.3% Triton X-100 (PBT), and

661   blocked in PBT + 5% BSA.

662   Antibodies used were: mouse anti-Wg (DSHB 1:50), mouse anti-Repo (DSHB 1:50),

663   mouse anti-Fz1 (DSHB 1:50), mouse anti-Fz2 (DSHB 1:50), Rabbit anti-Fz1 [103], 1:300),

664   mouse anti-Arm (DSHB 1:50), mouse anti-β-galactosidase (Sigma, 1:500), rabbit anti-

665   GFP (Invitrogen A11122, 1:500), mouse anti-GFP (Invitrogen A11120, 1:500), mouse

666   anti-Nc82 (DSHB 1:20), mouse anti-ELAV (DSHB 1:50), Rabbit anti-Hrp (Jackson

667   Immunoresearch 111-035-144, 1:400) , mouse anti-HA (12CA5 Roche 11583816001

668   1:100), rat anti-HA (Roche 11867423001, 1:200).

669   Secondary antibodies: anti-mouse Alexa 488, 647, anti-rabbit Alexa 488, 647

670   (Thermofisher, 1:500). DNA was stained with 2-(4-amidinophenyl)-1H-indole-6-

671   carboxamidine (DAPI, 1µM).

672

Cell culture, fixation and histology of S24 Xenograft model

673

674   The S24 cell line was derived as a primary glioblastoma culture (Lemke et al., 2012;

675   Osswald et al., 2015). For the S24 glioma model, 50.000 S24:GFP cells (stably

676   transduced by lentivirus) were injected into the cortex in 8-10 week old male NMRI

677   nude mice (Charles River, Sulzfeld, Germany, n=2). Cells were cultivated under serum-

678   free conditions in DMEM-F12 as sphere cultures (Thermo Fisher Scientific Inc.,

679   Waltham, MA, USA) supplemented with 2% B-27 (Thermo Fisher Scientific Inc.,

680   Waltham, MA, USA), 5 µg/ml human insulin (Sigma-Aldrich Corporation, St. Louis, MO,

681   USA), 12.8 ng/ml heparin (Sigma-Aldrich), 0.4 ng/ml EGF (R&D Systems Inc.,

682   Minneapolis, MN, USA) and 0.4 ng/ml FGF (Thermo Fisher Scientific Inc., Waltham,

27

683 MA, USA). Animals were sacrificed 90 days after glioma cell injection with age-

684 matched wild-type NMRI nude mice (n=2) which were used as control.

685 Brains were fixed with transcardial perfusion with 40 ml PBS and 40 ml 4 % PFA. The

686 brain was removed and postfixed in 4 % PFA for 4 hrs at room temperature. Afterwards

687 the brains were stored in PBS at 4 °C in the dark.

688 For histology, S24:GFP tumor-bearing brains were coronally cut on a vibratome

689 (Sigmann Elektronik, Hüffenhardt, Germany) into 100 µm sections. The sections were

690 permeabilized with 1 % TX100 for 3 hrs and counterstained with primary antibodies

691 against beta-catenin (abcam, ab32572) and WNT1 (abcam, ab15251) for 3 hrs in 0.2%

692 TX100 and 5 % FCS. Sections were washed three times with 0.2% TX100 and 5 %

693 FCS and counterstained with secondary antibodies couples to Alexa-647 and Alexa-

694 546 (Invitrogen) as well as DAPI for 3 hrs. The sections were washed three times in 1 ×

695 PBS, pH=7.4, and mounted on coverslips using self-made moviol. Images were

696 acquired on a confocal laser-scanning microscope (Leica SP8, Leica, Germany) using

697 a × 63 immersion oil objective (numeric aperture=1.4). z-Stacks were acquired with a

698 pixel size of 141 nm and 300-nm z-steps.

699 All animal experiments were approved by the regional animal welfare committee

700 (permit number: G132/16 Regierungspräsidium Karlsruhe).

701 **Western blots**

702 For western blots, we used NuPAGE Bis-Tris Gels 4–12% (Invitrogen), and the

703 following primary antibodies: mouse anti-Fz1 (DSHB 1:500), mouse anti-Fz2 (DSHB

704 1:500) and mouse anti-tubulin (1:10,000 Sigma), we use Tubulin as a loading control

705 instead of actin because the tumor microtubes are Actin positive and tubulin negative

706 as previously described [19]. There were 3 biological replicates and Relative Fz1

707 Average pixel intensity was measured using measurement tool from Image Studio Lite

708 Ver 5.2 and normalized against Tubulin.

709

Proximity ligation assay

710

711 DUO92101 Duolink® In Situ Red Starter Kit Mouse/Rabbit with DUO92013 Duolink In

712 Situ Detection Reagents FarRed (Sigma).

713 The interaction between Wg and Fz1 in Drosophila larval brains was detected *in situ*

714 accordingly to the instructions of the manufacturer. Briefly, primary antibody incubation

715 against Wg (mouse anti-Wg (DSHB 1:50) and Fz1 (Rabbit anti-Fz1 [103], 1:300)) were

716 applied using the same conditions as immunocytochemistry staining. Duolink

717 secondary antibodies against the primary antibodies were then added. These

718 secondary antibodies were provided as conjugates to oligonucleotides that were able

719 to form a closed circle via base pairing and ligation using Duolink ligation solution when

720 the antibodies were in close proximity [49] at a distance estimated to be <40 nm. The

721 detection of the signals was conducted by rolling circle amplification using DNA

722 polymerase incorporating fluorescently labeled nucleotides into the amplification

723 products. The resulting positive signals were visualized as bright fluorescent dots, with

724 each dot representing one interaction event. As negative control one of the primary

725 antibodies was not added therefore, no positive signals were obtained from that assay).

726 The tissues were visualized using a confocal microscope system (LEICA TCS SP5).

727

In situ hybridizations

728

729 Protocol was performed according to [104]. Imaginal discs and brains were dissected and

730 fixed in 4% formaldehyde for 20 min at room temperature, washed in PBS-0.1% Tween

731 (PBT) and re-fixed for 20 min at room temperature with 4% formaldehyde and 0.1%

732 Tween. After three washes in PBT, discs were stored at −20°C in hybridization solution

733 (HS; 50% formamide, 5× SSC, 100 μg/ml salmon sperm DNA, 50 μg/ml heparin and

734 0.1% Tween). Disc were pre-hybridized for 2 h at 55°C in HS and hybridized with

735 digoxigenin-labelled RNA probes at 55°C. The probes were previously denaturalized at

736 80°C for 10 min. After hybridization, discs were washed in HS and PBT, and

29

737   incubated for 2 h at room temperature in a 1:4000 dilution of anti-DIG antibody

738   (Roche). After incubation, the discs were washed in PBT and the detection of probes

739   was carried out using NBT and BCIP solution (Roche). The discs were mounted in 70%

740   glycerol. Images were acquired with a Leica DM750 microscope and Leica MC170HD

741   camera and LASv4.8 software. The probes were generated from the cDNAs RE026007

742   (*wg*) and LD32066 *(fz1)* from the Expression Sequence Tags (EST) collection of the

743   Berkeley Drosophila Genome Project.

744

745   **TEM**

746   Transmission electron microscopy (TEM) was performed in CNS of 3rd instar larvae

747   with horseradish peroxidase (HRP) genetically driven to glial cells. Brains were fixed in

748   4% formaldehyde in PBS for 30 min at room temperature, and washed in PBS,

749   followed by an amplification of HRP signal using the ABC kit (Vector Laboratories) at

750   room temperature. After developing with DAB brains were washed with PBS and fixed

751   with 2% glutaraldehyde, 4% formaldehyde in PBS for 2h at room temperature. After

752   washing in phosphate buffer the samples were postfixed with $OsO4$ 1% in 0.1 M

753   phosphate buffer, 1% $K3[Fe(CN)6]$ 1h at 4ºC. After washing in $dH2O$, Brains were

754   incubated with tannic acid in PBS for 1min at room temperature then washed in PBS

755   for 5min and $dH2O$ 2x5min. Then the samples were stained with 2% uranyl acetate in

756    $H2O$ for 1h at room temperature in darkness followed by 3 washes in $H2O2d$. . Brains

757   dehydrated in ethanol series (30%, 50%, 70%, 95%, 3x100% 10 min each at 4ºC).

758   Infiltration: samples were incubated in EtOH : propylene's OXID (1:1;V.V) for 5 min,

759   propylene's OXID 2x10min, propylene's OXID:Epon (1:1) for 45 min, Epon 100%   in

760   agitation for 1 h and Epon 100% in agitation overnight. Then change to Epon 100% for

761   2-3 h. Finally encapsulate the samples in BEEM capsules and polymerize 48h at

762   60ºC[105].

763

764   **Imaging**

765 Fluorescent labeled samples were mounted in Vectashield mounting media with DAPI

766 (Vector Laboratories) and analyzed by Confocal microscopy (LEICA TCS SP5/SP8).

767 Images were processed using Leica LAS AF Lite and Fiji (Image J 1.50e). Images were

768 assembled using Adobe Photoshop CS5.1.

769

770 **Quantifications and Statistical Analysis**

771 Relative Wg, Fz1, Arm, WNT1 and βCatenin staining within brains was determined

772 from images taken at the same confocal settings. Average pixel intensity was

773 measured using measurement log tool from Fiji 1.51g and Adobe Photoshop CS5.1.

774 Average pixel intensity was measured in the glial tissue and in the adjacent neuronal

775 tissue (N=~10 for each sample) and expressed as a ratio. Total average pixel intensity

776 of WNT1 and βCatenin staining within mice brains was measured in the glioma (N=6)

777 and control samples (N=6), to quantify this, single sections were taken from similar z-

778 positions in both control and glioma samples. Glial network volume was quantified

779 using Imaris surface tool (Imaris 6.3.1 software). The number of Proximity ligation

780 assay puncta, HA$^+$ puncta, Repo$^+$ cells and the number of synaptic active sites was

781 quantified by using the Imaris 6.3.1 software.

782 The Western Blot bands were quantified by using the Image Studio Lite 5.2 software.

783 Data was analyzed and plotted using GraphPad Prism v7.0.0. A D'Agostino & Pearson

784 normality test was performed and the data found to have a normal distribution were

785 analyzed by a two-tailed t-test with Welch-correction. In the case of multiple

786 comparisons a One-way ANOVA with bonferroni post test was used. The data that did

787 not pass the normality test were submitted to a two-tailed Mann-Whitney U-test or in

788 the case of multiple comparisons a Kruskal-Wallis test with Dunns post test. Error bars

789 represent Standard Error of the Mean, significance was ***p≤0.0001, ** p≤0.001 *

790 p≤0.01, ns=non-significant.

791

792

31

Viability assays

Flies were crossed and progeny was raised at 25ºC under standard conditions. The number of adult flies emerged from the pupae were counted for each genotype. The number of control flies was considered 100% viability and all genotypes are represented relative to controls. Experiments were performed in triplicates.

Survival assay

Males *Tub-Gal80; Repo-Gal4* were crossed with males bearing a control construct (*UAS–LacZ*) or glioma (*UAS–PI3K^{dp110}; UAS-EGFR$^{\lambda}$*) and raised at 17°C. Progeny bearing a glioma (experimental) or LacZ (control) chromosomes were put at 29ºC and viability was calculated as the percentage of surviving flies with respect to the starting number of flies as follows: viability = observed (nº of flies)/starting nº of flies × 100. Six independent vials for glioma (*n*= 6) and control (*n*= 6) were analyzed, with each vial with 10 flies.

qRT-PCRs

Total RNA was isolated from larvae brains (Trizol, Invitrogen) and cDNAs were synthesized with M-MLV RT (Invitrogen). The following specific probes from applied Biosystems were used: Wingless Dm01814379_m1 and Frizzled1 Dm01793718_g1, RpL32 Dm02151827_g1 was used as housekeeping.

qRT-PCR was performed using Taqman Gene Expression (Applied Biosystems) using a 7500 Real Time PCR System (Applied Biosystems) with cycling conditions of 95°C for 10 min and 40 cycles of 95°C for 15 s and 55°C for 1 min. Each experimental point was performed with samples from two independent crosses and three replicates per experimental point, and differences were assessed with a 2-tailed Student *t* test. Results were normalized using the housekeeping RpL32 and the ΔΔ cycle threshold method and are expressed as the relative change (-fold) of the stimulated group over

819   the control group, which was used as a calibrator. qRT-PCR results were analyzed with

820   7500 v2.0.6 software (Applied Biosystems).

821

822   **Figure Legends**

823   **Figure 1: Co-activation of EGFR-Ras and PI3K in *Drosophila* glia causes an**

824   **expansion of the glial network**

825   Brains from 3rd instar larvae. Glia nuclei are labeled with GFP^{NLS} (green) driven by

826   *repo-Gal4*. Each brain is composed of 2 symmetrical hemispheres. (A-C) In

827   *repo>dEGFR$^\lambda$; dp110^{CAAX}* (*glioma*) larvae (B), both brain hemispheres are enlarged and

828   elongated and the number of glial cells is increased relative to *wt* control (A). Lower

829   magnifications are shown in A´ and b´. The quantification of the number of glial cells is

830   shown in (C). Arrows indicate glial nuclei.

831   (D–E) Optical sections of larval brain to visualize the glial network, glial cell bodies and

832   membranes are labeled in red (myrRFP). (D) RFP signal in control brains shows glial

833   somas and the network in *wt* brain. (E) The glioma brain shows a dramatic increase in

834   the membrane projections and in the size of the network. Nuclei are marked with DAPI

835   (blue).

836   (F-L) Transmission electron microscopy (TEM) images of a 3rd instar larval brains

837   expressing HRP in the glial cells. (F-G) HRP deposits label cell profiles membranes in

838   dark, thus identifying glial cells. Coloured images from control brains showing glial cells

839   identified by HRP staining (magenta) and HRP-negative neurons (cyan). (H) Schematic

840   diagram, a glioma cell labeled with HRP (magenta) showing that glioma cells produce a

841   network of TMs that grow to surround neighboring neurons (cyan). (I-L) Several

842   magnifications of Glioma brains showing TMs that grow and enwrap neighboring

33

843   neurons (cyan). Detail of several layers of a glioma membrane enwrapping a neuron

844   (K-L) and a longitudinal section of a TM (J), arrows indicate glial membranes.

845   (M-P) Glia are labeled with *UAS-ihog-RFP* to visualize active cytoneme/TM structures

846   in glial cells as part of an interconnecting network. (M) In control brains the active glial

847   cytonemes are shown by *repo>ihog-RFP* in red. In glioma brains (N), the TMs grow

848   and expand across the brain, quantification of the network volume (O) and the

849   network/glial cell ratio is shown in P.

850   (Q) Glia is labeled with *UAS-Ihog-RFP* driven by *repo-Gal4* to visualize TMs in glial

851   cells, nuclei are marked with DAPI (blue) and Neurons are stained in green (Hrp) and

852   enwrapped by glial TMs in glioma brains (yellow arrowheads). (R) Glia is labeled with

853   *UAS-myr-RFP* driven by *repo-Gal4* to visualize membrane projections in glial cells,

854   nuclei are marked with DAPI (blue) and Neurons are stained in green (ELAV) and

855   enwrapped by glial TMs in glioma brains (yellow arrowheads). Error bars show S.D. ***

856   P<0.0001. Scale bar size are indicated in this and all figures. Genotypes: (A) w; *repo-*

857   *Gal4, UAS-GFP^{nls}/UAS-lacZ,* (B) *UAS-dEGFR$^\lambda$, UAS-dp110^{CAAX};; repo-Gal4, UAS-*

858   *GFP^{nls},* (D) w; *Gal80^{ts}; repo-Gal4, UAS-myrRFP/UAS-lacZ,* (E, R) *UAS-dEGFR$^\lambda$, UAS-*

859   *dp110^{CAAX}; Gal80^{ts}; repo-Gal4, UAS-myrRFP,* (F-G) w; *UAS-HRP:CD2; repo-*

860   *Gal4/UAS-lacZ,* (I-L) *UAS-dEGFR$^\lambda$, UAS-dp110^{CAAX}; UAS-HRP:CD2; repo-Gal4,* (M)

861   w;; *repo-Gal4, UAS-ihog-RFP/UAS-lacZ,* (N, Q) *UAS-dEGFR$^\lambda$, UAS-dp110^{CAAX};; repo-*

862   *Gal4, UAS-ihog-RFP*

863

864   **Figure 2: Wingless/Fz1 accumulate in glioma cells**

865   Larval brain sections with glial cell bodies and membranes labeled in red (myrRFP) and

866   stained with Wg antibody show homogeneous expression in the control brains (A) in

867   green. In the glioma brains Wg accumulates in the glial transformed cells (B), the Wg

868   average pixel intensity ratio between Glia/Neuron quantification is shown in (C). Arrows

34

869   indicate Wg staining in glial membranes. (D-F) Glial cells are labeled with *UAS-Ihog-*

870   *RFP* to visualize the glial network, and stained with Fz1 (green). (D) Fz1 is

871   homogeneously distributed in control brains, with a slight accumulation in the Ihog+

872   structures. (E) Fz1 accumulates in the TMs and specifically in the projections that are

873   in contact with the neuronal clusters. (F) Upon knockdown of *fz1* in glioma brains, the

874   tumoral glial network is still formed but Fz1 is not detectable. (G) Knockdown of *igl* in

875   glioma brains restores a normal glial network and Fz1 shows a homogeneous

876   distribution along the brain section. Arrows indicate Fz1 staining in glial membranes.

877   (H) Fz1 average pixel intensity ratio between Glia/Neuron quantification ⁻. Nuclei are

878   marked with DAPI. Error bars show S.D. * P<0.01 *** P<0.0001. Genotypes: (A) w;

879   *Gal80^{ts}; repo-Gal4, UAS-myrRFP/UAS-lacZ*, (B) *UAS-dEGFR^{λ}, UAS-dp110^{CAAX};*

880   *Gal80^{ts}; repo-Gal4, UAS-myrRFP*, (C) w;; *repo-Gal4, ihog-RFP/UAS-lacZ*, (D) *UAS-*

881   *dEGFR^{λ}, UAS-dp110^{CAAX};; repo-Gal4, UAS-ihog-RFP*, (E) *UAS-dEGFR^{λ}, UAS-*

882   *dp110^{CAAX}; UAS-Fz1-RNAi; repo-Gal4, UAS-ihog-RFP*, (F) *UAS-dEGFR^{λ}, UAS-*

883   *dp110^{CAAX};; repo-Gal4, UAS-ihog-RFP /UAS-igl-RNAi*

884

885   **Figure 3: Fz1 in glia interacts with neuronal Wg**

886   GRASP technique was used and both halves of green fluorescent protein tagged with a

887   CD4 signal to direct it to the membranes (CD4-spGFP) were expressed in neurons

888   (*elav-lexA*) and glial (*repo-Gal4*) cells respectively. Only upon intimate contact GFP

889   protein is reconstituted and green fluorescent signal is visible. (A-C) Control brains

890   showed a discrete signal corresponding to the physiological interaction between glia

891   and neurons. (D-F) In glioma brains a massive GFP signal from GRASP reporter is

892   detected. Arrows indicate GRASP reconstitution GFP signal. (G-H) Proximity ligation

893   assays (PLA) were performed in control and glioma brains to quantify the interactions

894   between Wg and Fz1. (G) Control brains showed a discrete number of puncta (green)

895   showing the physiological interactions. (H) Glioma brains showed a five-fold increase in

896   the number of puncta, quantified in (I). The number of PLA+ Wg-Fz1 interactions per

897   Repo+ cell in control and glioma brains is shown in (J). Nuclei are marked with DAPI

898   (blue). Arrows indicate PLA$^+$ puncta. Error bars show S.D. *** P<0.0001. Genotypes:

899   (A-C) w;; *elav-lexA; repo-Gal4, UAS-ihog-RFP/UAS-CD4-spGFP1-10, lexAop-CD4-*

900   *spGFP11,* (D-F) *UAS-dEGFR$^{\lambda}$, UAS-dp110^{CAAX}; elav-lexA; repo-Gal4, UAS-ihog-RFP/*

901   *UAS-CD4-spGFP1-10, lexAop-CD4-spGFP11,* (G) w;; *repo-Gal4, ihog-RFP/UAS-lacZ,*

902   (H) *UAS-dEGFR$^{\lambda}$, UAS-dp110^{CAAX};; repo-Gal4, UAS-ihog-RFP*

903

904   **Figure 4: Wg signaling pathway is active in glioma cells, and the glioma**

905   **inactivates it in neuronal clusters in glioma brains.**

906   Larval brain sections with glial cytonemes labeled in red and stained with Arm (green).

907   (A) Cytoplasmic-Armadillo (Cyt-Arm) is homogeneously distributed in control sections.

908   (B) In glioma brains Cyt-Arm accumulates in the neurons cytoplasm where it is inactive.

909   (C) Knockdown of *igl* in glioma brains restores a normal glial network and Arm does not

910   accumulate showing a homogeneous distribution similar to the control. Arrows indicate

911   Cyt-Arm staining at the Glia-neuron interphase. (D) Cyt-Arm average pixel intensity

912   ratio between Neuron/Glia quantification showing the Wg signaling pathway silencing in

913   neurons in a glioma brain. Glial cell bodies and membranes are labeled with myrRFP

914   (red). (E-H) Wg signaling pathway reporters *arm-GFP* (E-F) and *nkd-lacZ* (stained with

915   anti-bGal (G-H) in control and glioma brains show activation of the pathway in glioma

916   cells compared with the reporter activation mostly in neurons in the control brains.

917   Arrows indicate cells with reporter activation. (I-N) Confocal immunofluorescence single

918   plane images of S24 GBSC NMRI nude mice brains (glioma) and NMRI nude mice

919   (control) brains stained with human anti-βCatenin (I-J) and WNT1 (L-M) both show in

920   grey (red in the merged image) an increase in the glioma samples. The corresponding

921 quantification of the pixel intensity is shown in K and N. Green signal from tumor cell

922 GFP expression allows specific detection of S24 GBSC related structures in the mouse

923 brain (I´, L´). Arrows indicate glioma or control cells. Nuclei are marked with DAPI.

924 Error bars show S.D. *** P<0.0001 and ns for non-significant. Genotypes: (A) w;; *repo-*

925 *Gal4, ihog-RFP/UAS-lacZ,* (B) *UAS-dEGFR$^\lambda$, UAS-dp110^{CAAX};; repo-Gal4, UAS-ihog-*

926 *RFP,* (C) *UAS-dEGFR$^\lambda$, UAS-dp110^{CAAX};; repo-Gal4, UAS-ihog-RFP /UAS-igl-RNAi,*

927 (E) *w; Gal80^{ts}; repo-Gal4, UAS-myrRFP/ arm-GFP,* (F) *UAS-dEGFR$^\lambda$, UAS-dp110^{CAAX};*

928 *Gal80^{ts}; repo-Gal4, UAS-myrRFP/ arm-GFP,* (G) *w; Gal80^{ts}; repo-Gal4, UAS-*

929 *myrRFP/nkd04869a-lacZ,* (H) *UAS-dEGFR$^\lambda$, UAS-dp110^{CAAX}; Gal80^{ts}; repo-Gal4, UAS-*

930 *myrRFP/nkd04869a-lacZ*

931

932 **Figure 5: Glioma network is responsible for the increase in the number of glial**

933 **cells.**

934 Larval brain sections with glial cell nuclei stained with Repo (green). The number of

935 glial cells is quantified in the following genotypes: (A) Control, (B) Glioma showing an

936 increase in Repo+ cells. (C) Upon knockdown of *Fz1* in glioma brains, the number of

937 glial cells is partially restored (D) knockdown of *igl* in glioma brains restores the number

938 of glial cells similar to the control. (E) Quantification of the number of Repo+ cells.

939 Nuclei are marked by DAPI (blue). (F) Viability assay showing the % lethality induced

940 by the glioma that is partially rescued upon knockdown of *fz1*. Error bars show S.D. ***

941 P<0.0001, and ns for non-significant. Genotypes: (A) w;; *repo-Gal4, ihog-RFP/UAS-*

942 *lacZ,* (B) *UAS-dEGFR$^\lambda$, UAS-dp110^{CAAX};; repo-Gal4, UAS-ihog-RFP,* (C) *UAS-dEGFR$^\lambda$,*

943 *UAS-dp110^{CAAX}; UAS-Fz1-RNAi; repo-Gal4, UAS-ihog-RFP,* (D) *UAS-dEGFR$^\lambda$, UAS-*

944 *dp110^{CAAX};; repo-Gal4, UAS-ihog-RFP /UAS-igl-RNAi,* (F) 1. w;; *repo-Gal4, ihog-*

945 *RFP/UAS-lacZ 2.* w; *UAS-fz1-RNAi; repo-Gal4, UAS-ihog-RFP 3.UAS-dEGFR$^\lambda$, UAS-*

37

946   *dp110^{CAAX};; repo-Gal4, UAS-ihog-RFP   4. UAS-dEGFR$^\lambda$, UAS-dp110^{CAAX}; UAS-fz1-*

947   *RNAi; repo-Gal4, UAS-ihog-RFP*

948

949   **Figure 6: Gliomas cause Neurodegeneration and Wg expression in glioma cells**

950   **is dispensable for tumor progression**

951   Neurons from the larval neuromuscular junction are stained with Nc82 showing the

952   synaptic active zones. (A-F) Upon glioma induction (B) the number of synapses (grey)

953   is reduced when compared with the control (A). The number of synapses is restored

954   upon knockdown of *Fz1* (C), *igl* (D) or *armS10; Fz1-RNAi* (E).The quantification of

955   synapse number in all genotypes is shown in (F). (G-L) *wg* knockdown (I) in glioma

956   cells (*wg-RNAi*) or *armS10; Fz1-RNAi* (J) does not prevent glioma cell numbers

957   increase nor glioma TMs volume expansion quantified in (K-L). Error bars show S.D.

958   *** P<0.0001, ** P<0.001 and ns for non-significant. Genotypes: (A, G) w;; *repo-Gal4,*

959   *ihog-RFP/UAS-lacZ,* (B, H) *UAS-dEGFR$^\lambda$, UAS-dp110^{CAAX};; repo-Gal4, UAS-ihog-RFP,*

960   (C) *UAS-dEGFR$^\lambda$, UAS-dp110^{CAAX}; UAS-Fz1-RNAi; repo-Gal4, UAS-ihog-RFP,* (D)

961   *UAS-dEGFR$^\lambda$, UAS-dp110^{CAAX};; repo-Gal4, UAS-ihog-RFP /UAS-igl-RNAi,* (E, J) *UAS-*

962   *arm^{S10}/UAS-dEGFR$^\lambda$, UAS-dp110^{CAAX}; UAS-Fz1-RNAi; repo-Gal4, UAS-ihog-RFP,* (I)

963   *UAS-dEGFR$^\lambda$, UAS-dp110^{CAAX}; UAS-wg-RNAi; repo-Gal4, UAS-ihog-RFP*

964

965   **Figure 7: Knockdown of the Wg signaling pathway results in neurodegeneration**

966   **and restoration of the glia-neuron Wg/Fz1 signaling equilibrium inhibits glioma**

967   **progression.**

968   Neurons from the larval neuromuscular junction are stained with Nc82 showing the

969   synaptic active Zones. (A-D) Upon knockdown of *wg* (C) or *Fz1* in D42 neurons (B) the

970   number of synapses (grey) is reduced when compared with the control (A). Arrows

971   indicate synapses. The quantification of synapse number in all genotypes is shown in

972   (D).

973   (E-H) Larval brain sections with glial network labeled with *UAS-Ihog-RFP* in red and

974   stained with Fz1 (grey or blue in the merge). Neurons are labeled with *lexAop-CD8-*

975   *GFP* driven by *elav-lexA*. Fz1 overexpression in neurons (green) restore homogeneous

976   Fz1 protein distribution (blue) in the brain, rescue brain size and neuron distribution (G

977   and magnification in H) compared to (E and magnification in F) where the *elav-lexA* is

978   not present in the glioma brains, Nuclei are marked with DAPI in (E-F) (green). Arrows

979   indicate Fz1 staining in the glial membranes at the Glia-neuron interphase of glioma

980   brains and its restored localization in G-H.

981   (I-L) Neurons from the larval neuromuscular junction are stained with Nc82 showing the

982   active Zones. Upon glioma induction the number of synapses (grey) is reduced (J)

983   when compared with the control (I). The number of synapses is restored upon

984   overexpression of Fz1 specifically in the neurons (K). Arrows indicate synapses. The

985   quantification of synapse number is shown in (L). Error bars show S.D. *** P<0.0001, *

986   P<0.01 or ns for non-significant. Genotypes: (A) w; *UAS-CD8-GFP; D42-Gal4/UAS-*

987   *lacZ,* (B) w; *UAS-CD8-GFP/Fz1-RNAi; D42-Gal4,* (C) w; *UAS-CD8-GFP/wg-RNAi;*

988   *D42-Gal4,* (E-F, J) *UAS-dEGFR$^\lambda$, UAS-dp110^{CAAX}; lexAop-Fz1; repo-Gal4, UAS-ihog-*

989   *RFP,* (G-H, K) *UAS-dEGFR$^\lambda$, UAS-dp110^{CAAX}; lexAop-fz1/ elav-lexA, lexAop-CD8-GFP;*

990   *repo-Gal4, UAS-ihog-RFP,* (I) w; *repo-Gal4, ihog-RFP/UAS-lacZ*

991

992   **Figure 8: Glioma depletes Wg from neuronal membrane**

993

994   Larval brain sections with glial network labeled with *UAS-Ihog-RFP* in red and stained

995   with HA (blue). (A, magnification in B, H) Control brains express Wg^{NRT}-HA and the

996   anti-HA (grey or blue in the merge) staining shows a positive signal in both neurons

997 (green) and glial cells (red). (C-D) Glioma samples that do not express Wg^{NRT} in

998 neurons do not show HA nor GFP signal. (E, magnification in F, I) Glioma brains with

999 membrane anchored Wg (Wg^{NRT}-HA grey or blue in the merge) in neurons (green),

1000 show a homogeneous signal for HA (grey or blue in the merge) in both glioma cells and

1001 neurons, quantified in (J), and the glial network volume size is restored in these

1002 animals (K). Arrows indicate HA^{+} staining in glial or neuronal membranes. Error bars

1003 show S.D. *** P<0.0001,   ns for non-significant. (G) Schematic diagram of this

1004 experiment: a neuron labeled with GFP (green) and a glioma cell labeled with ihog-

1005 RFP (red) showing that glioma cells produce a network of TMs that grow to reach

1006 neighboring neurons. Intimate membrane contact facilitates neuronal-Wg (blue)

1007 sequestering mediated by Fz1 receptor (black) from glioma. In this experiment neurons

1008 express a membrane anchored version of Wg (Wg^{NRT} represented as Wg in blue with a

1009 purple anchor) which is more difficult for the glioma to retrieve from the neuron.

1010 Genotypes: (A-B, H) w; *>wg>wgNRT-HA, PaxRFP/ elav-lexA, lexAop-CD8-GFP; repo-*

1011 *Gal4, UAS-ihog-RFP/lexAop-flp,* (C-D) *UAS-dEGFR$^{\lambda}$, UAS-dp110^{CAAX}; >wg>wgNRT-*

1012 *HA, PaxRFP ; repo-Gal4, UAS-ihog-RFP/lexAop-flp,* (E-F, I) *UAS-dEGFR$^{\lambda}$, UAS-*

1013 *dp110^{CAAX}; >wg>wgNRT-HA, PaxRFP/ elav-lexA, lexAop-CD8-GFP; repo-Gal4, UAS-*

1014 *ihog-RFP/lexAop-flp*

1015

1016 **Supplementary Figures and VideosFigure S1 (Related to Figure 1): TMs enwrap**

1017 **neurons in GB and cytoneme markers co-localize with glioma network**

1018 (A-B) Control and glioma brains from 3rd instar larvae. Glia is labeled with *UAS-Ihog-*

1019 *RFP* driven by *repo-Gal4* to visualize TMs in glial cells as part of an interconnecting

1020 network (red). Glial network is marked with lifeActin-GFP reporter (green) and nuclei

1021 are marked with DAPI (blue). Imaris 3D reconstructions are shown in A´´´-B´´´).

1022   (C-G) Glial network is marked with several cytoneme markers: (C) lifeact-GFP reporter

1023   (green and glial nuclei are marked with Repo, magenta), (D) GMA-GFP (green), (E)

1024   GPI-YFP (green), (F) GFP-MLC (green), (G) sqh-GFP (green) in a glioma brain. (H-I)

1025   Downregulation of neuroglian (*nrg-RNAi*) in glioma brains results in defective TMs.

1026   (J-M) Higher magnifications of control brains (J) showing the glial cytonemes (red)

1027   compared with the glioma brains where the TMs overgrow and enwrap neuronal

1028   clusters (K). Upon *igl/Gap43* downregulation the glial network does not overgrow or

1029   enwrap neuronal clusters (L) and shows a pattern and size similar to the control.

1030   Nuclei are marked with DAPI. Arrows indicate glial cytonemes/TMs. (M) A viability

1031   assay shows that the lethality induced by the glioma is fully rescued upon knockdown

1032   of *Gap43/igl*. Nuclei are marked with DAPI. Scale bar size are indicated in this and all

1033   figures. Genotypes: **Figure S1**

1034   (A) *w; lifeActin-GFP; repo-Gal4, UAS-ihog-RFP/UAS-lacZ,* (B-C) *UAS-dEGFR$^\lambda$, UAS-*

1035   *dp110^{CAAX}; lifeActin-GFP; repo-Gal4, UAS-ihog-RFP,* (D) *UAS-dEGFR$^\lambda$, UAS-*

1036   *dp110^{CAAX}; UAS-GMA-GFP; repo-Gal4, UAS-ihog-RFP,* (E) *UAS-dEGFR$^\lambda$, UAS-*

1037   *dp110^{CAAX}; UAS-GPI-YFP/Gal80^{ts}; repo-Gal4, UAS-myrRFP,* (F) *UAS-dEGFR$^\lambda$, UAS-*

1038   *dp110^{CAAX}; Gal80^{ts}; repo-Gal4, UAS-myrRFP/ UAS-GFP-sls(MLC),* (G) *UAS-dEGFR$^\lambda$,*

1039   *UAS-dp110^{CAAX}; Gal80^{ts}; repo-Gal4, UAS-myrRFP/ Sqh-GFP,* (H-I) *UAS-dEGFR$^\lambda$,*

1040   *UAS-dp110^{CAAX}; UAS-nrg-RNAi; repo-Gal4, UAS-ihog-RFP,* (J) *w; repo-Gal4, UAS-*

1041   *ihog-RFP/UAS-lacZ,* (K) *UAS-dEGFR$^\lambda$, UAS-dp110^{CAAX};; repo-Gal4, UAS-ihog-RFP,*

1042   (L) *UAS-dEGFR$^\lambda$, UAS-dp110^{CAAX};; repo-Gal4, UAS-ihog-RFP /UAS-igl-RNAi*

1043

1044   **Figure S2 (Related to Figure 1): igl/*Gap43* Knockdown does not show effects in**

1045   **the number of synapses in the NMJ, in the glial network or in the viability of the**

1046   **flies**

41

1047   (A-B) Glial cells are stained with Repo (green) and the number of glial cells are

1048   quantified in the following genotypes: *Control*, *Glioma* showing an increase in Repo+

1049   cells, *Glioma;lacZ* and *Glioma;yellow-RNAi* showing a similar number of Repo+ cells to

1050   Glioma alone. (C-D) Upon *igl* knockdown by *RNAi* in normal brains, the glial network is

1051   similar to the control. Glial cells are marked by Repo in green. Nuclei are marked by

1052   DAPI. (E-F) Neurons from the larval neuromuscular junction are stained with Nc82

1053   showing the synaptic active sites. Upon knockdown of *igl* the number of synapses

1054   marked by Nc82 (green) is similar to the control. (F) Graph showing the quantification

1055   of the synapse number. (G) A viability assay shows that the knockdown of *igl* does not

1056   alter the % viability of male and female flies. Error bars show S.D. *** P<0.0001 or ns

1057   for non-significant. Genotypes: (A) *UAS-dEGFR$^\lambda$, UAS-dp110^{CAAX}; UAS-yellow-RNAi;*

1058   *repo-Gal4, UAS-ihog-RFP,* (B) 1. *w; repo-Gal4, ihog-RFP/UAS-lacZ* 2. *UAS-dEGFR$^\lambda$,*

1059   *UAS-dp110^{CAAX};; repo-Gal4, UAS-ihog-RFP* 3. *UAS-dEGFR$^\lambda$, UAS-dp110^{CAAX}; UAS-*

1060   *lacZ; repo-Gal4, UAS-ihog-RFP* 4. *UAS-dEGFR$^\lambda$, UAS-dp110^{CAAX}; UAS-yellow-RNAi;*

1061   *repo-Gal4, UAS-ihog-RFP,* (C-D) *w; repo-Gal4, UAS-ihog-RFP/UAS-igl-RNAi,* (E-F) 1.

1062   *w; UAS-CD8-GFP; D42-Gal4/UAS-igl-RNAi* 2. *w; UAS-CD8-GFP; D42-Gal4/UAS-lacZ,*

1063   (G) 1. *w; repo-Gal4, UAS-ihog-RFP/UAS-lacZ* 2. *w; repo-Gal4, UAS-ihog-RFP/UAS-igl-*

1064   *RNAi*

1065

1066   **Figure S3 (Related to Figure 2): Cases of human GB patients with mutations in**

1067   **WNT or FZD.**

1068   Complete analysis of mutations in human GB samples from COSMIC database

1069   http://cancer.sanger.ac.uk/cosmic (A) and Cancer Genome Atlas (TGAC) for

1070   transcriptional targets of WNT pathway (B), WNT ligands (C) and FZD receptors (D),

1071   data are represented in percentage out of 902 or 922 samples. The total number of

42

1072   cases with mutations in any WNT or FZD gene is shown in red. Genes from WNT and

1073   FZD family without mutations in GBs is shown in the bottom.

1074

1075   **Figure S4 (Related to Figure 2): Fz2 remains normal in glioma brains.**

1076   (A) Wing imaginal control disc stained with Fz2 (green) showing the expected

1077   endogenous localization pattern. Brains from 3rd instar larvae displayed at the same

1078   scale. Glia is labeled with *UAS-Ihog-RFP* driven by *repo-Gal4* to visualize active

1079   filopodia/TMs in glial cells, and stained with Fz2 (green). (B) Fz2 is homogeneously

1080   distributed in control sections, (C) Fz2 is homogeneously distributed in glioma brain

1081   sections, similar to the control. Nuclei are marked by DAPI (blue). Scale bar size is

1082   indicated in the figure. Glial cell bodies and membranes are labeled with *UAS-myrRFP*

1083   (red) driven by *repo-Gal4* and stained with GFP antibody to visualize a tagged form of

1084   endogenous Fz1 protein. Genotypes: (A) *w; UAS-lacZ,* (B) *w;; repo-Gal4, ihog-*

1085   *RFP/UAS-lacZ,* (C) *UAS-dEGFR$^{\lambda}$, UAS-dp110^{CAAX};; repo-Gal4, UAS-ihog-RFP*

1086

1087   **Figure S5 (Related to Figure 2 and 7): Validation of tools, RNAis and antibodies**

1088   (A) *UAS-Fz1-RNAi* tool was validated in epithelial tissue, wing imaginal discs. Upon

1089   *UAS-Fz1-RNAi* expression in the posterior compartment (marked with GFP), there is a

1090   reduction in Fz1 protein signal compared with the anterior compartment from the same

1091   tissue. (B) *UAS-Wg-RNAi* tool was validated in epithelial tissue, wing imaginal discs.

1092   Upon *UAS-Wg-RNAi* expression in the posterior compartment (marked with GFP),

1093   there is a reduction in Wg protein signal compared with the anterior compartment from

1094   the same tissue. (C) *lexAop-Fz1* tool was validated in brain tissue. Upon ectopic Fz1

1095   expression in the neurons (driven by *ELAV-LexA* marked with GFP), there is an

1096   increase in Fz1 protein signal compared with the rest of the brain tissue. (D) Upon

43

1097   ectopic Fz1 expression in the neurons (driven by *ELAV-LexA>lexAop-Fz1* marked with

1098   GFP), there is an increase in active Arm protein signal compared with the rest of the

1099   brain tissue.

1100   Genotypes: (A) w; *Gal80^{ts}/UAS-Fz1-RNAi; en-Gal4, UAS-GFP,* (B) w; *Gal80^{ts}/UAS-wg-*

1101   *RNAi; en-Gal4, UAS-GFP,* (C-E) w; *lexAop-fz1/ elav-lexA, lexAop-CD8-GFP*

1102

1103   **Figure S6 (Related to Figure 3): Wg and Fz1 transcription levels are similar**

1104   **between controls and gliomas**

1105   (A) qPCRs with *RNA* extracted from control and glioma larvae showing no change in

1106   the transcription (*mRNA* levels)of *wg* or *fz1*. (B) Western blot of samples extracted from

1107   control and glioma larvae showing no change in the amount of Fz1 or Fz2 protein.

1108   Error bars show S.D. ns for non-significant. (C) In situ hybridization experiments for Wg

1109   and Fz1 in controls and gliomas showing no change in the transcription (*mRNA* levels)

1110   of *wg* or *fz1. Genotypes:* (A-C) 1. *w;; repo-Gal4, ihog-RFP/UAS-lacZ* 2. *UAS-dEGFR^{λ},*

1111   *UAS-dp110^{CAAX};; repo-Gal4, UAS-ihog-RFP*

1112

1113   **Figure S7 (Related to Figure 4): Wg signaling pathway is active in glioma cells**

1114   Larval brain sections with glial network labeled in red and stained with Cyt-Arm (green).

1115   (A) Knockdown of *Fz1* in glioma brains showing a homogeneous Cyt-Arm distribution

1116   similar to the control. Quantification of Cyt-Arm staining ratio between Ihog+ and Ihog⁻

1117   domains is shown in principal Figure 5D. (B-G) Glial cell bodies and membranes are

1118   labeled with myrRFP or ihog-RFP (red) driven by *repo-Gal4*. Wg signaling pathway

1119   reporters *tsh-lacZ* stained with anti-bGal (B-C), *fz4-GFP* (D-E) and *dally-lacZ* stained

1120   with anti-bGal (F-G) show activation of the pathway in glial transformed cells.

1121   Genotypes: (A) *UAS-dEGFR^{λ}, UAS-dp110^{CAAX}; UAS-Fz1-RNAi; repo-Gal4, UAS-ihog-*

1122   *RFP,* (B) *w;; repo-Gal4, UAS-myrRFP/tsh-lacZ,* (C) *UAS-dEGFR^{λ}, UAS-dp110^{CAAX};;*

1123   *repo-Gal4, UAS-myrRFP/tsh-lacZ,* (D) *w;; repo-Gal4, UAS-myrRFP/ fz4-GFP,* (E) *UAS-*

1124   *dEGFR$^{\lambda}$, UAS-dp110^{CAAX};; repo-Gal4, UAS-myrRFP/ fz4-GFP,* (F) *w;; repo-Gal4, UAS-*

1125   *myrRFP/ dally-lacZ,* (G) *UAS-dEGFR$^{\lambda}$, UAS-dp110^{CAAX};; repo-Gal4, UAS-myrRFP/*

1126   *dally-lacZ*

1127

1128   **Figure S8 (Related to Figure 4): Wg signaling pathway is active in human glioma**

1129   **cells**

1130   (A-D) A series of grade II and III GB images from S24 xenografts brain sections stained

1131   with WNT1 and ß-Catenin show an increase of these signals in grade III when

1132   compared with grade II brain sections, indicating that the accumulation of WNT1 and ß-

1133   Catenin correlates with the progression of the GB, quantified in (E-F) (G-H) Technical

1134   immunohistofluorescence negative control in NMRI nude control mice brains stained

1135   only with the corresponding secondary antibodies showing the background unspecific

1136   signal. Nuclei are marked by DAPI (blue).

1137   **Figure S9 (Related to Figure 2, 4 and 6): Adult *Drosophila* gliomas**

1138   (A) Survival curve of adult control or glioma flies after a number of days of glioma

1139   induction and progression. (B-H) Adult brain sections 7 days after glioma induction with

1140   Glial cells are labeled with *UAS-myr-RFP* to visualize the glial network and stained with

1141   Cyt-Arm, Fz1 and Wg antibodies. (B-C, D) Cyt-Arm staining specifically marks the

1142   mushroom bodies and it is homogeneously distributed in the rest of the brain tissue in

1143   control sections and accumulates in the neurons cytoplasm where it is inactive in

1144   glioma brains. Quantification of Neuron/Glia Cyt-Arm staining ratio between RFP+ and

1145   RFP^{-} domains (D). (B´-C´, E) Fz1 staining show homogeneous localization in the

1146   control brains (B´) in blue. In the glioma brains Fz1 accumulates in the glial

1147   transformed cells (C´), Glia/Neuron Fz1 average pixel intensity ratio quantification is

1148   shown in (E). (F-H) Wg is homogeneously distributed in control brains, with a slight

1149   accumulation in the RFP+ structures. Wg accumulates in the glioma network similar to

1150   the larval brains. Glia/Neuron Wg average pixel intensity ratio quantification is shown in

1151   (H). (I) Graph showing synapse number quantification of adult NMJs from control flies

1152   and glioma-bearing flies. Error bars show S.D. *** P<0.0001 or ns for non-significant.

1153   Genotypes: (B, F) w; *Gal80^{ts}; repo-Gal4, UAS-myrRFP/UAS-lacZ,* (C, G) *UAS-dEGFR$^{\lambda}$,*

1154   *UAS-dp110^{CAAX}; Gal80^{ts}; repo-Gal4, UAS-myrRFP*

1155

1156   **Figure S10 (Related to Figure 7): Restoration of the glia-neuron Wg/Fz1 signaling**

1157   **equilibrium inhibits glioma progression**

1158   (A-D) Brains from 3rd instar larvae displayed at the same scale. Glia is labeled with

1159   *UAS-lhog-RFP* driven by *repo-Gal4* to visualize active filopodia in glial cells, and

1160   stained with Wg or Cyt-Arm (green). Neurons are labeled with *lexAop-CD8-GFP* driven

1161   by *elav-lexA* (blue). Fz1 overexpression in neurons (blue) restore homogeneous Wg

1162   (grey or green in the merge) (B) and Cyt-Arm (D) protein distribution (green) in the

1163   brain, compared to (A, C) where the *elav-lexA* is not present in the glioma brains,

1164   Nuclei are marked by DAPI (blue) in (A, C). Genotypes: (A, C) *UAS-dEGFR$^{\lambda}$, UAS-*

1165   *dp110^{CAAX}; lexAop-Fz1; repo-Gal4, UAS-ihog-RFP,* (B, D) *UAS-dEGFR$^{\lambda}$, UAS-*

1166   *dp110^{CAAX}; lexAop-Fz1/ elav-lexA, lexAop-CD8-GFP; repo-Gal4, UAS-ihog-RFP*

1167

1168   **Video S1: Control Network**

1169   3D video reconstruction of control brains with glia labeled with *ihog-RFP* (*repo>ihog-*

1170   *RFP*) in red (grey in the 3D reconstruction) to visualize cytoneme structures in glial

1171   cells as part of an interconnecting network.

1172

1173   **Video S2: Glioma TMs**

46

1174   3D video reconstruction of Glioma brains with glia labeled with *ihog-RFP* (*repo>ihog-*

1175   *RFP*) in red (grey in the 3D reconstruction) to visualize TMs structures in glial cells as

1176   part of an interconnecting network. In glioma brains, the TMs expand across the brain

1177   and form perineuronal nests.

1178

1179   **Video S3: Glioma *igl-RNAi* Network**

1180   3D video reconstruction of Glioma; *igl-RNAi* brains with glia labeled with *ihog-RFP*

1181   (*repo>ihog-RFP*) in red (grey in the 3D reconstruction) to visualize TM structures in

1182   glial cells as part of an interconnecting network. Upon *igl* downregulation the glial

1183   network does not overgrow or enwrap neuronal clusters and shows a pattern and size

1184   similar to the control.

1185

1186   **Video S4: Control LifeActin**

1187   3D video reconstruction of control brains from 3rd instar larvae. Glia is labeled with

1188   *UAS-Ihog-RFP* driven by *repo-Gal4* to visualize cytonemes in glial cells as part of an

1189   interconnecting network (red). Glial network is marked with lifeActin-GFP reporter

1190   (green) and nuclei are marked with DAPI (blue).

1191

1192   **Video S5: Glioma LifeActin**

1193   3D video reconstruction of gliomal brains from 3rd instar larvae. Glia is labeled with

1194   *UAS-Ihog-RFP* driven by *repo-Gal4* to visualize TMs in glial cells as part of an

1195   interconnecting network (red). Glial network is marked with lifeActin-GFP reporter

1196   (green) and nuclei are marked with DAPI (blue). Glial TMs enwrap clusters of neurons

1197   in individual GB perineuronal nests.

1198

1199 **Video S6: Climbing assay**

1200 Video of *Drosophila* adult negative geotaxis behavior analysis (climbing assay), as an

1201 indication for possible motor defects associated with neurodegeneration. The results

1202 showed symptoms of neurodegeneration in glioma flies (right tube) compared to

1203 controls (left tube).

1204

1205

1206 1 Bi, W. L. & Beroukhim, R. Beating the odds: extreme long-term survival with
1207 glioblastoma. *Neuro Oncol* **16**, 1159-1160, doi:nou166 [pii]
1208 10.1093/neuonc/nou166 (2014).
1209 2 Messaoudi, K., Clavreul, A. & Lagarce, F. Toward an effective strategy in glioblastoma
1210 treatment. Part I: resistance mechanisms and strategies to overcome resistance of
1211 glioblastoma to temozolomide. *Drug Discov Today* **20**, 899-905, doi:S1359-
1212 6446(15)00080-X [pii]
1213 10.1016/j.drudis.2015.02.011 (2015).
1214 3 Belhadj, Z. *et al.* Multifunctional targeted liposomal drug delivery for efficient
1215 glioblastoma treatment. *Oncotarget*, doi:17976 [pii]
1216 10.18632/oncotarget.17976 (2017).
1217 4 Xu, Y. Y., Gao, P., Sun, Y. & Duan, Y. R. Development of targeted therapies in treatment
1218 of glioblastoma. *Cancer Biol Med* **12**, 223-237, doi:10.7497/j.issn.2095-3941.2015.0020
1219 cbm-12-03-223 [pii] (2015).
1220 5 Zhu, Y. *et al.* Bi-specific molecule against EGFR and death receptors simultaneously
1221 targets proliferation and death pathways in tumors. *Sci Rep* **7**, 2602,
1222 doi:10.1038/s41598-017-02483-9
1223 10.1038/s41598-017-02483-9 [pii] (2017).
1224 6 Osuka, S. & Van Meir, E. G. Overcoming therapeutic resistance in glioblastoma: the
1225 way forward. *J Clin Invest* **127**, 415-426, doi:89587 [pii]
1226 10.1172/JCI89587 (2017).
1227 7 Shtutman, M. *et al.* The cyclin D1 gene is a target of the beta-catenin/LEF-1 pathway.
1228 *Proc Natl Acad Sci U S A* **96**, 5522-5527 (1999).
1229 8 He, T. C. *et al.* Identification of c-MYC as a target of the APC pathway. *Science* **281**,
1230 1509-1512 (1998).
1231 9 Loh, K. M., van Amerongen, R. & Nusse, R. Generating Cellular Diversity and Spatial
1232 Form: Wnt Signaling and the Evolution of Multicellular Animals. *Dev Cell* **38**, 643-655,
1233 doi:10.1016/j.devcel.2016.08.011 (2016).
1234 10 Oliva, C. A., Vargas, J. Y. & Inestrosa, N. C. Wnts in adult brain: from synaptic plasticity
1235 to cognitive deficiencies. *Front Cell Neurosci* **7**, 224, doi:10.3389/fncel.2013.00224
1236 (2013).
1237 11 Inestrosa, N. C. & Varela-Nallar, L. Wnt signaling in the nervous system and in
1238 Alzheimer's disease. *J Mol Cell Biol* **6**, 64-74, doi:10.1093/jmcb/mjt051 (2014).

12   Arnes, M. & Casas Tinto, S. Aberrant Wnt signaling: a special focus in CNS diseases. *J Neurogenet*, 1-7, doi:10.1080/01677063.2017.1338696 (2017).

13   Paul, I., Bhattacharya, S., Chatterjee, A. & Ghosh, M. K. Current Understanding on EGFR and Wnt/beta-Catenin Signaling in Glioma and Their Possible Crosstalk. *Genes Cancer* **4**, 427-446, doi:10.1177/1947601913503341 10.1177_1947601913503341 [pii] (2013).

14   Qiu, X., Jiao, J., Li, Y. & Tian, T. Overexpression of FZD7 promotes glioma cell proliferation by upregulating TAZ. *Oncotarget* **7**, 85987-85999, doi:13292 [pii] 10.18632/oncotarget.13292 (2016).

15   Suwala, A. K., Hanaford, A., Kahlert, U. D. & Maciaczyk, J. Clipping the Wings of Glioblastoma: Modulation of WNT as a Novel Therapeutic Strategy. *J Neuropathol Exp Neurol* **75**, 388-396, doi:nlw013 [pii] 10.1093/jnen/nlw013 (2016).

16   Liu, C. *et al.* Wnt/beta-Catenin pathway in human glioma: expression pattern and clinical/prognostic correlations. *Clin Exp Med* **11**, 105-112, doi:10.1007/s10238-010-0110-9 (2011).

17   Sareddy, G. R., Panigrahi, M., Challa, S., Mahadevan, A. & Babu, P. P. Activation of Wnt/beta-catenin/Tcf signaling pathway in human astrocytomas. *Neurochem Int* **55**, 307-317, doi:S0197-0186(09)00123-5 [pii] 10.1016/j.neuint.2009.03.016 (2009).

18   Rheinbay, E. *et al.* An aberrant transcription factor network essential for Wnt signaling and stem cell maintenance in glioblastoma. *Cell Rep* **3**, 1567-1579, doi:S2211-1247(13)00203-9 [pii] 10.1016/j.celrep.2013.04.021 (2013).

19   Osswald, M. *et al.* Brain tumour cells interconnect to a functional and resistant network. *Nature* **528**, 93-98, doi:nature16071 [pii] 10.1038/nature16071 (2015).

20   Weil, S. *et al.* Tumor microtubes convey resistance to surgical lesions and chemotherapy in gliomas. *Neuro Oncol* **19**, 1316-1326, doi:3738031 [pii] 10.1093/neuonc/nox070 (2017).

21   Lou, E. *et al.* Imaging Tunneling Membrane Tubes Elucidates Cell Communication in Tumors. *Trends Cancer* **3**, 678-685, doi:S2405-8033(17)30158-9 [pii] 10.1016/j.trecan.2017.08.001 (2017).

22   Ramirez-Weber, F. A. & Kornberg, T. B. Cytonemes: cellular processes that project to the principal signaling center in Drosophila imaginal discs. *Cell* **97**, 599-607, doi:S0092-8674(00)80771-0 [pii] (1999).

23   Kornberg, T. B. Distributing signaling proteins in space and time: the province of cytonemes. *Curr Opin Genet Dev* **45**, 22-27, doi:S0959-437X(16)30219-2 [pii] 10.1016/j.gde.2017.02.010 (2017).

24   Read, R. D., Cavenee, W. K., Furnari, F. B. & Thomas, J. B. A drosophila model for EGFR-Ras and PI3K-dependent human glioma. *PLoS Genet* **5**, e1000374, doi:10.1371/journal.pgen.1000374 (2009).

25   Read, R. D. *et al.* A kinome-wide RNAi screen in Drosophila Glia reveals that the RIO kinases mediate cell proliferation and survival through TORC2-Akt signaling in glioblastoma. *PLoS Genet* **9**, e1003253, doi:10.1371/journal.pgen.1003253 PGENETICS-D-12-01408 [pii] (2013).

26   Yao, S., Lum, L. & Beachy, P. The ihog cell-surface proteins bind Hedgehog and mediate pathway activation. *Cell* **125**, 343-357, doi:10.1016/j.cell.2006.02.040 (2006).

27   Callejo, A. *et al.* Dispatched mediates Hedgehog basolateral release to form the long-range morphogenetic gradient in the Drosophila wing disk epithelium. *Proc Natl Acad Sci U S A* **108**, 12591-12598, doi:1106881108 [pii] 10.1073/pnas.1106881108 (2011).

1291   28   Bischoff, M. *et al.* Cytonemes are required for the establishment of a normal
1292   Hedgehog morphogen gradient in Drosophila epithelia. *Nat Cell Biol* **15**, 1269-1281,
1293   doi:10.1038/ncb2856 (2013).
1294   29   Holland, E. C. Glioblastoma multiforme: the terminator. *Proc Natl Acad Sci U S A* **97**,
1295   6242-6244, doi:97/12/6242 [pii] (2000).
1296   30   Roy, S., Huang, H., Liu, S. & Kornberg, T. B. Cytoneme-mediated contact-dependent
1297   transport of the Drosophila decapentaplegic signaling protein. *Science* **343**, 1244624,
1298   doi:science.1244624 [pii]
1299   10.1126/science.1244624 (2014).
1300   31   Neel, V. A. & Young, M. W. Igloo, a GAP-43-related gene expressed in the developing
1301   nervous system of Drosophila. *Development* **120**, 2235-2243 (1994).
1302   32   Campos, B., Olsen, L. R., Urup, T. & Poulsen, H. S. A comprehensive profile of recurrent
1303   glioblastoma. *Oncogene* **35**, 5819-5825, doi:onc201685 [pii]
1304   10.1038/onc.2016.85 (2016).
1305   33   Venkatesan, S., Lamfers, M. L., Dirven, C. M. & Leenstra, S. Genetic biomarkers of drug
1306   response for small-molecule therapeutics targeting the RTK/Ras/PI3K, p53 or Rb
1307   pathway in glioblastoma. *CNS Oncol* **5**, 77-90, doi:10.2217/cns-2015-0005 (2016).
1308   34   Kahlert, U. D. *et al.* Pharmacologic Wnt Inhibition Reduces Proliferation, Survival, and
1309   Clonogenicity of Glioblastoma Cells. *J Neuropathol Exp Neurol* **74**, 889-900,
1310   doi:10.1097/NEN.0000000000000227 (2015).
1311   35   Paw, I., Carpenter, R. C., Watabe, K., Debinski, W. & Lo, H. W. Mechanisms regulating
1312   glioma invasion. *Cancer Lett* **362**, 1-7, doi:S0304-3835(15)00195-0 [pii]
1313   10.1016/j.canlet.2015.03.015 (2015).
1314   36   Zheng, H. *et al.* PLAGL2 regulates Wnt signaling to impede differentiation in neural
1315   stem cells and gliomas. *Cancer Cell* **17**, 497-509, doi:S1535-6108(10)00147-9 [pii]
1316   10.1016/j.ccr.2010.03.020 (2010).
1317   37   Kim, Y. *et al.* Wnt activation is implicated in glioblastoma radioresistance. *Lab Invest*
1318   **92**, 466-473, doi:labinvest2011161 [pii]
1319   10.1038/labinvest.2011.161 (2012).
1320   38   Kamino, M. *et al.* Wnt-5a signaling is correlated with infiltrative activity in human
1321   glioma by inducing cellular migration and MMP-2. *Cancer Sci* **102**, 540-548,
1322   doi:10.1111/j.1349-7006.2010.01815.x (2011).
1323   39   Pu, P. *et al.* Downregulation of Wnt2 and beta-catenin by siRNA suppresses malignant
1324   glioma cell growth. *Cancer Gene Ther* **16**, 351-361, doi:cgt200878 [pii]
1325   10.1038/cgt.2008.78 (2009).
1326   40   Lee, Y., Lee, J. K., Ahn, S. H., Lee, J. & Nam, D. H. WNT signaling in glioblastoma and
1327   therapeutic opportunities. *Lab Invest* **96**, 137-150, doi:labinvest2015140 [pii]
1328   10.1038/labinvest.2015.140 (2016).
1329   41   Jin, X. *et al.* Frizzled 4 regulates stemness and invasiveness of migrating glioma cells
1330   established by serial intracranial transplantation. *Cancer Res* **71**, 3066-3075, doi:0008-
1331   5472.CAN-10-1495 [pii]
1332   10.1158/0008-5472.CAN-10-1495 (2011).
1333   42   Lee, Y. *et al.* FoxM1 Promotes Stemness and Radio-Resistance of Glioblastoma by
1334   Regulating the Master Stem Cell Regulator Sox2. *PLoS One* **10**, e0137703,
1335   doi:10.1371/journal.pone.0137703
1336   PONE-D-15-20790 [pii] (2015).
1337   43   Nager, M. *et al.* beta-Catenin Signalling in Glioblastoma Multiforme and Glioma-
1338   Initiating Cells. *Chemother Res Pract* **2012**, 192362, doi:10.1155/2012/192362 (2012).
1339   44   Wang, Z., Zhang, S., Siu, T. L. & Huang, S. Glioblastoma multiforme formation and EMT:
1340   role of FoxM1 transcription factor. *Curr Pharm Des* **21**, 1268-1271, doi:CPD-EPUB-
1341   63931 [pii] (2015).

45   Zhang, N. *et al.* FoxM1 promotes beta-catenin nuclear localization and controls Wnt target-gene expression and glioma tumorigenesis. *Cancer Cell* **20**, 427-442, doi:S1535-6108(11)00312-6 [pii]
10.1016/j.ccr.2011.08.016 (2011).

46   Denysenko, T. *et al.* WNT/beta-catenin Signaling Pathway and Downstream Modulators in Low- and High-grade Glioma. *Cancer Genomics Proteomics* **13**, 31-45, doi:13/1/31 [pii] (2016).

47   Schilling, S., Steiner, S., Zimmerli, D. & Basler, K. A regulatory receptor network directs the range and output of the Wingless signal. *Development* **141**, 2483-2493, doi:10.1242/dev.108662 (2014).

48   Feinberg, E. H. *et al.* GFP Reconstitution Across Synaptic Partners (GRASP) defines cell contacts and synapses in living nervous systems. *Neuron* **57**, 353-363, doi:S0896-6273(07)01020-3 [pii]
10.1016/j.neuron.2007.11.030 (2008).

49   Soderberg, O. *et al.* Direct observation of individual endogenous protein complexes in situ by proximity ligation. *Nat Methods* **3**, 995-1000, doi:nmeth947 [pii]
10.1038/nmeth947 (2006).

50   Koos, B. *et al.* Analysis of protein interactions in situ by proximity ligation assays. *Curr Top Microbiol Immunol* **377**, 111-126, doi:10.1007/82_2013_334 (2014).

51   Klaus, A. & Birchmeier, W. Wnt signalling and its impact on development and cancer. *Nat Rev Cancer* **8**, 387-398, doi:nrc2389 [pii]
10.1038/nrc2389 (2008).

52   Riggleman, B., Schedl, P. & Wieschaus, E. Spatial expression of the Drosophila segment polarity gene armadillo is posttranscriptionally regulated by wingless. *Cell* **63**, 549-560, doi:0092-8674(90)90451-J [pii] (1990).

53   Singh, A., Kango-Singh, M. & Sun, Y. H. Eye suppression, a novel function of teashirt, requires Wingless signaling. *Development* **129**, 4271-4280 (2002).

54   DasGupta, R., Kaykas, A., Moon, R. T. & Perrimon, N. Functional genomic analysis of the Wnt-wingless signaling pathway. *Science* **308**, 826-833, doi:10.1126/science.1109374 (2005).

55   Franz, A., Shlyueva, D., Brunner, E., Stark, A. & Basler, K. Probing the canonicity of the Wnt/Wingless signaling pathway. *PLoS Genet* **13**, e1006700, doi:10.1371/journal.pgen.1006700
PGENETICS-D-17-00130 [pii] (2017).

56   Scherer, H. J. A Critical Review: The Pathology of Cerebral Gliomas. *J Neurol Psychiatry* **3**, 147-177 (1940).

57   Peng, F. *et al.* Loss of Polo ameliorates APP-induced Alzheimer's disease-like symptoms in Drosophila. *Sci Rep* **5**, 16816, doi:srep16816 [pii]
10.1038/srep16816 (2015).

58   Keshishian, H., Broadie, K., Chiba, A. & Bate, M. The drosophila neuromuscular junction: a model system for studying synaptic development and function. *Annu Rev Neurosci* **19**, 545-575, doi:10.1146/annurev.ne.19.030196.002553 (1996).

59   Mhatre, S. D. *et al.* Synaptic abnormalities in a Drosophila model of Alzheimer's disease. *Dis Model Mech* **7**, 373-385, doi:dmm.012104 [pii]
10.1242/dmm.012104 (2014).

60   Penney, J. *et al.* LRRK2 regulates retrograde synaptic compensation at the Drosophila neuromuscular junction. *Nat Commun* **7**, 12188, doi:ncomms12188 [pii]
10.1038/ncomms12188 (2016).

61   Boyle, M., Bonini, N. & DiNardo, S. Expression and function of clift in the development of somatic gonadal precursors within the Drosophila mesoderm. *Development* **124**, 971-982 (1997).

62   Arrazola, M. S., Silva-Alvarez, C. & Inestrosa, N. C. How the Wnt signaling pathway protects from neurodegeneration: the mitochondrial scenario. *Front Cell Neurosci* **9**, 166, doi:10.3389/fncel.2015.00166 (2015).

63   Garcia-Velazquez, L. & Arias, C. The emerging role of Wnt signaling dysregulation in the understanding and modification of age-associated diseases. *Ageing Res Rev* **37**, 135-145, doi:S1568-1637(17)30090-9 [pii]
10.1016/j.arr.2017.06.001 (2017).

64   Kahn, M. Can we safely target the WNT pathway? *Nat Rev Drug Discov* **13**, 513-532, doi:nrd4233 [pii]
10.1038/nrd4233 (2014).

65   Libro, R., Bramanti, P. & Mazzon, E. The role of the Wnt canonical signaling in neurodegenerative diseases. *Life Sci* **158**, 78-88, doi:S0024-3205(16)30380-0 [pii]
10.1016/j.lfs.2016.06.024 (2016).

66   Casas-Tinto, S., Arnes, M. & Ferrus, A. Drosophila enhancer-Gal4 lines show ectopic expression during development. *R Soc Open Sci* **4**, 170039, doi:10.1098/rsos.170039
rsos170039 [pii] (2017).

67   Lai, S. L. & Lee, T. Genetic mosaic with dual binary transcriptional systems in Drosophila. *Nat Neurosci* **9**, 703-709, doi:10.1038/nn1681 (2006).

68   Bejsovec, A. & Martinez Arias, A. Roles of wingless in patterning the larval epidermis of Drosophila. *Development* **113**, 471-485 (1991).

69   Alexandre, C., Baena-Lopez, A. & Vincent, J. P. Patterning and growth control by membrane-tethered Wingless. *Nature* **505**, 180-185, doi:10.1038/nature12879 (2014).

70   Zecca, M., Basler, K. & Struhl, G. Direct and long-range action of a wingless morphogen gradient. *Cell* **87**, 833-844 (1996).

71   Venkatesh, H. S. *et al.* Neuronal Activity Promotes Glioma Growth through Neuroligin-3 Secretion. *Cell* **161**, 803-816, doi:S0092-8674(15)00429-8 [pii]
10.1016/j.cell.2015.04.012 (2015).

72   Johung, T. & Monje, M. Neuronal activity in the glioma microenvironment. *Curr Opin Neurobiol* **47**, 156-161, doi:S0959-4388(17)30058-2 [pii]
10.1016/j.conb.2017.10.009 (2017).

73   Qin, E. Y. *et al.* Neural Precursor-Derived Pleiotrophin Mediates Subventricular Zone Invasion by Glioma. *Cell* **170**, 845-859 e819, doi:S0092-8674(17)30823-1 [pii]
10.1016/j.cell.2017.07.016 (2017).

74   Jung, E. *et al.* Tweety-Homolog 1 Drives Brain Colonization of Gliomas. *J Neurosci* **37**, 6837-6850, doi:JNEUROSCI.3532-16.2017 [pii]
10.1523/JNEUROSCI.3532-16.2017 (2017).

75   Bergo, E. *et al.* Cognitive Rehabilitation in Patients with Gliomas and Other Brain Tumors: State of the Art. *Biomed Res Int* **2016**, 3041824, doi:10.1155/2016/3041824 (2016).

76   Bosma, I. *et al.* The course of neurocognitive functioning in high-grade glioma patients. *Neuro Oncol* **9**, 53-62, doi:10.1215/15228517-2006-012 (2007).

77   Brown, P. D. *et al.* Detrimental effects of tumor progression on cognitive function of patients with high-grade glioma. *J Clin Oncol* **24**, 5427-5433, doi:10.1200/JCO.2006.08.5605 (2006).

78   Wefel, J. S. *et al.* Neurocognitive function in patients with recurrent glioblastoma treated with bevacizumab. *Neuro Oncol* **13**, 660-668, doi:10.1093/neuonc/nor024 (2011).

79   Gehrke, A. K., Baisley, M. C., Sonck, A. L., Wronski, S. L. & Feuerstein, M. Neurocognitive deficits following primary brain tumor treatment: systematic review of a decade of comparative studies. *J Neurooncol* **115**, 135-142, doi:10.1007/s11060-013-1215-2 (2013).

80   Henstridge, C. M., Pickett, E. & Spires-Jones, T. L. Synaptic pathology: A shared mechanism in neurological disease. *Ageing Res Rev* **28**, 72-84, doi:10.1016/j.arr.2016.04.005 (2016).

81   Hong, S. *et al.* Complement and microglia mediate early synapse loss in Alzheimer mouse models. *Science* **352**, 712-716, doi:10.1126/science.aad8373 (2016).

82   Sephton, C. F. & Yu, G. The function of RNA-binding proteins at the synapse: implications for neurodegeneration. *Cell Mol Life Sci* **72**, 3621-3635, doi:10.1007/s00018-015-1943-x (2015).

83   Mansilla, A. *et al.* Interference of the complex between NCS-1 and Ric8a with phenothiazines regulates synaptic function and is an approach for fragile X syndrome. *Proc Natl Acad Sci U S A* **114**, E999-E1008, doi:10.1073/pnas.1611089114 (2017).

84   Romero-Pozuelo, J. *et al.* The guanine-exchange factor Ric8a binds to the Ca(2)(+) sensor NCS-1 to regulate synapse number and neurotransmitter release. *J Cell Sci* **127**, 4246-4259, doi:10.1242/jcs.152603 (2014).

85   John Lin, C. C. *et al.* Identification of diverse astrocyte populations and their malignant analogs. *Nat Neurosci* **20**, 396-405, doi:10.1038/nn.4493 (2017).

86   Salter, M. W. & Stevens, B. Microglia emerge as central players in brain disease. *Nat Med* **23**, 1018-1027, doi:nm.4397 [pii]
10.1038/nm.4397 (2017).

87   Niikura, T., Tajima, H. & Kita, Y. Neuronal cell death in Alzheimer's disease and a neuroprotective factor, humanin. *Curr Neuropharmacol* **4**, 139-147 (2006).

88   Ye, Z. C., Rothstein, J. D. & Sontheimer, H. Compromised glutamate transport in human glioma cells: reduction-mislocalization of sodium-dependent glutamate transporters and enhanced activity of cystine-glutamate exchange. *J Neurosci* **19**, 10767-10777 (1999).

89   Lee, S. G. *et al.* Oncogene AEG-1 promotes glioma-induced neurodegeneration by increasing glutamate excitotoxicity. *Cancer Res* **71**, 6514-6523, doi:0008-5472.CAN-11-0782 [pii]
10.1158/0008-5472.CAN-11-0782 (2011).

90   Robert, S. M. *et al.* SLC7A11 expression is associated with seizures and predicts poor survival in patients with malignant glioma. *Sci Transl Med* **7**, 289ra286, doi:7/289/289ra86 [pii]
10.1126/scitranslmed.aaa8103 (2015).

91   Kornberg, T. B. Cytonemes extend their reach. *EMBO J* **32**, 1658-1659, doi:emboj2013115 [pii]
10.1038/emboj.2013.115 (2013).

92   Kornberg, T. B. & Roy, S. Cytonemes as specialized signaling filopodia. *Development* **141**, 729-736, doi:141/4/729 [pii]
10.1242/dev.086223 (2014).

93   Sherer, N. M. & Mothes, W. Cytonemes and tunneling nanotubes in cell-cell communication and viral pathogenesis. *Trends Cell Biol* **18**, 414-420, doi:S0962-8924(08)00190-6 [pii]
10.1016/j.tcb.2008.07.003 (2008).

94   Neumann-Giesen, C. *et al.* Membrane and raft association of reggie-1/flotillin-2: role of myristoylation, palmitoylation and oligomerization and induction of filopodia by overexpression. *Biochem J* **378**, 509-518, doi:10.1042/BJ20031100 (2004).

95   Watts, R. J., Schuldiner, O., Perrino, J., Larsen, C. & Luo, L. Glia engulf degenerating axons during developmental axon pruning. *Curr Biol* **14**, 678-684, doi:10.1016/j.cub.2004.03.035
S0960-9822(04)00214-3 [pii] (2004).

1494   96   Greco, V., Hannus, M. & Eaton, S. Argosomes: a potential vehicle for the spread of
1495   morphogens through epithelia. *Cell* **106**, 633-645, doi:S0092-8674(01)00484-6 [pii]
1496   (2001).
1497   97   Bloor, J. W. & Kiehart, D. P. zipper Nonmuscle myosin-II functions downstream of PS2
1498   integrin in Drosophila myogenesis and is necessary for myofibril formation. *Dev Biol*
1499   **239**, 215-228, doi:10.1006/dbio.2001.0452
1500   S0012-1606(01)90452-X [pii] (2001).
1501   98   Furnari, F. B. *et al.* Malignant astrocytic glioma: genetics, biology, and paths to
1502   treatment. *Genes Dev* **21**, 2683-2710, doi:21/21/2683 [pii]
1503   10.1101/gad.1596707 (2007).
1504   99   Maher, E. A. *et al.* Malignant glioma: genetics and biology of a grave matter. *Genes Dev*
1505   **15**, 1311-1333, doi:10.1101/gad.891601 (2001).
1506   100   Kegelman, T. P. *et al.* In vivo modeling of malignant glioma: the road to effective
1507   therapy. *Adv Cancer Res* **121**, 261-330, doi:B978-0-12-800249-0.00007-X [pii]
1508   10.1016/B978-0-12-800249-0.00007-X (2014).
1509   101   Read, R. D. Drosophila melanogaster as a model system for human brain cancers. *Glia*
1510   **59**, 1364-1376, doi:10.1002/glia.21148 (2011).
1511   102   Brand, A. H. & Perrimon, N. Targeted gene expression as a means of altering cell fates
1512   and generating dominant phenotypes. *Development* **118**, 401-415 (1993).
1513   103   Bastock, R. & Strutt, D. The planar polarity pathway promotes coordinated cell
1514   migration during Drosophila oogenesis. *Development* **134**, 3055-3064,
1515   doi:10.1242/dev.010447 (2007).
1516   104   Martin, M., Ostale, C. M. & de Celis, J. F. Patterning of the Drosophila L2 vein is driven
1517   by regulatory interactions between region-specific transcription factors expressed in
1518   response to Dpp signalling. *Development* **144**, 3168-3176, doi:dev.143461 [pii]
1519   10.1242/dev.143461 (2017).
1520   105   Martin-Pena, A. *et al.* Cell types and coincident synapses in the ellipsoid body of
1521   Drosophila. *Eur J Neurosci* **39**, 1586-1601, doi:10.1111/ejn.12537 (2014).
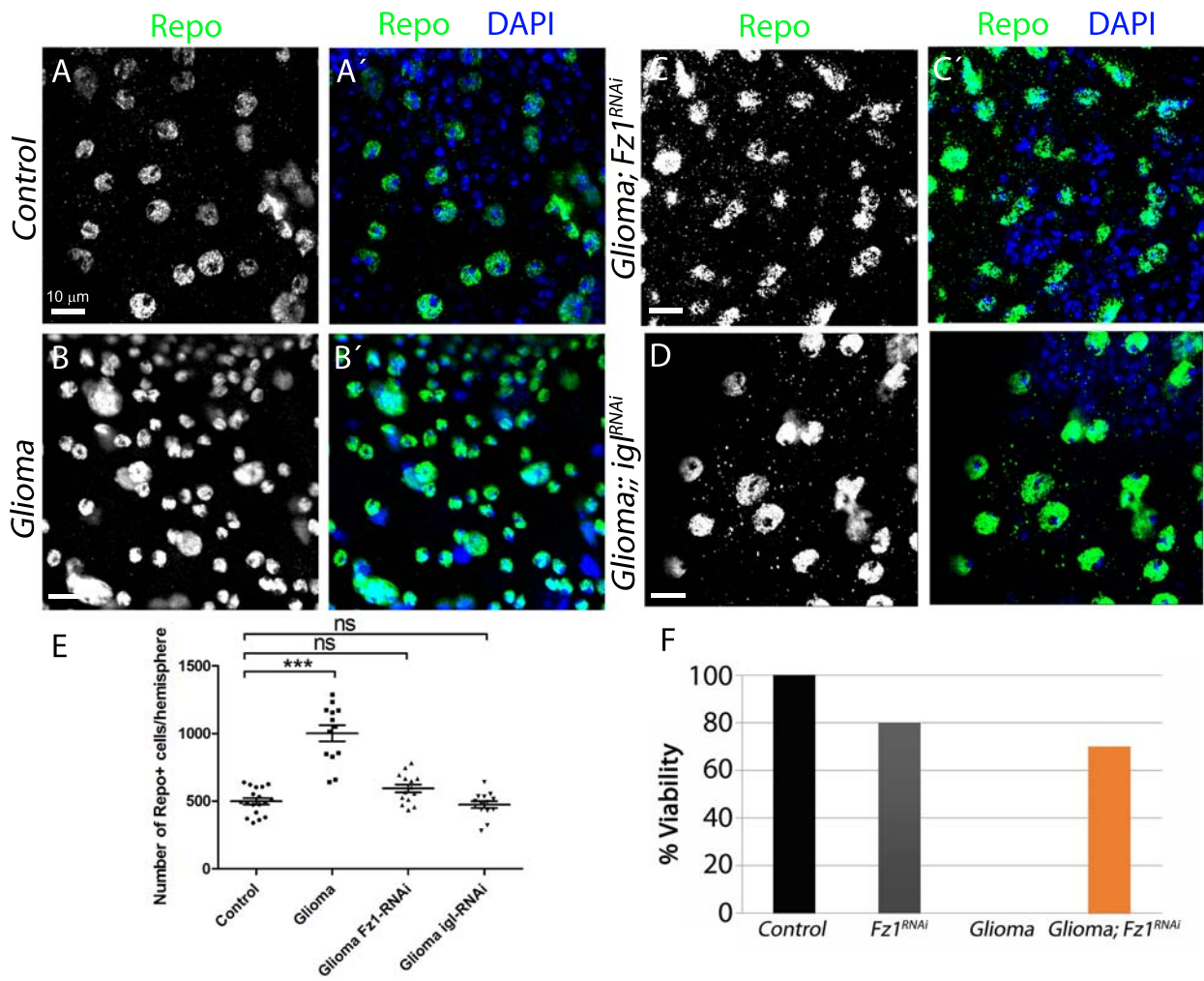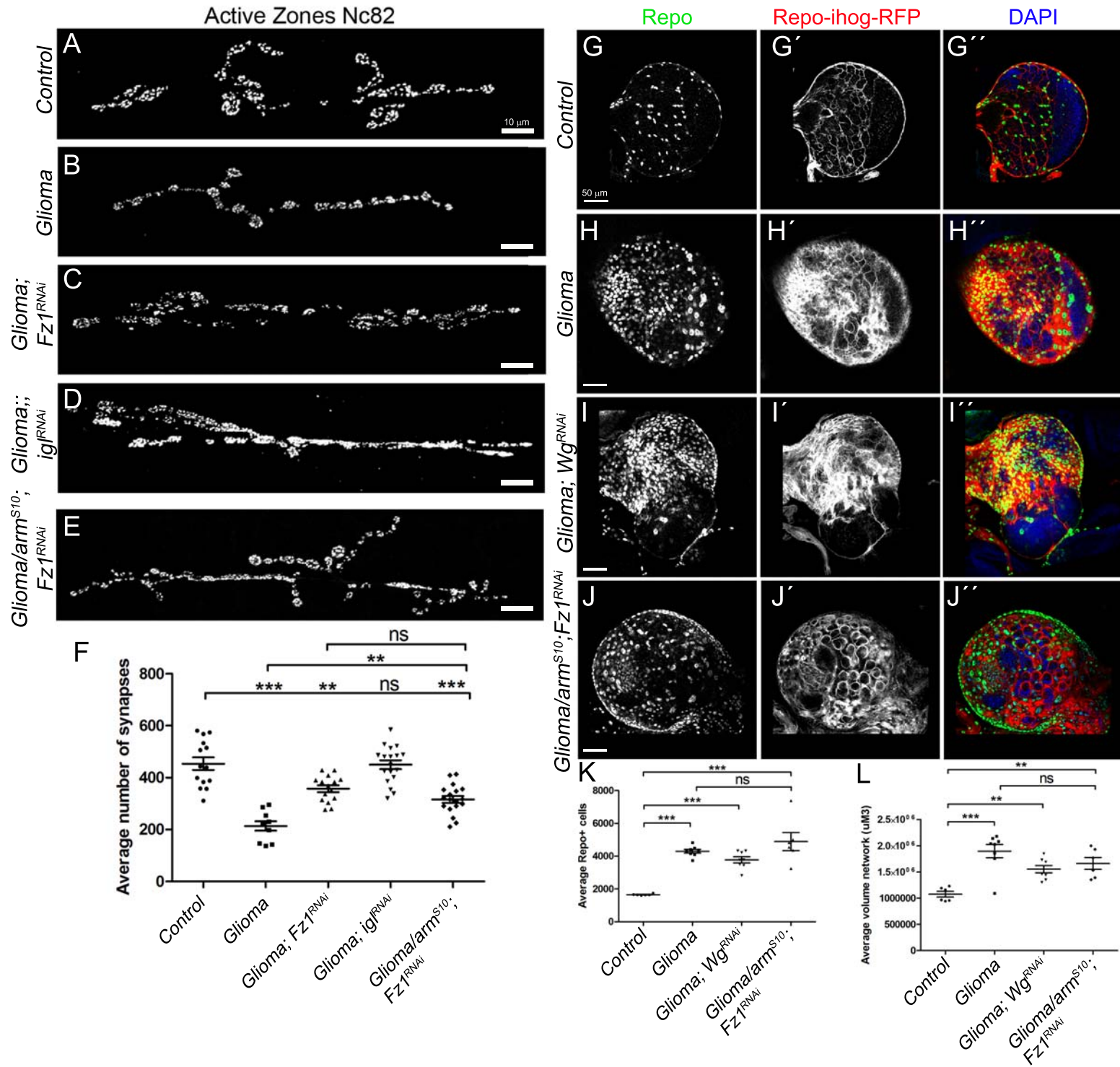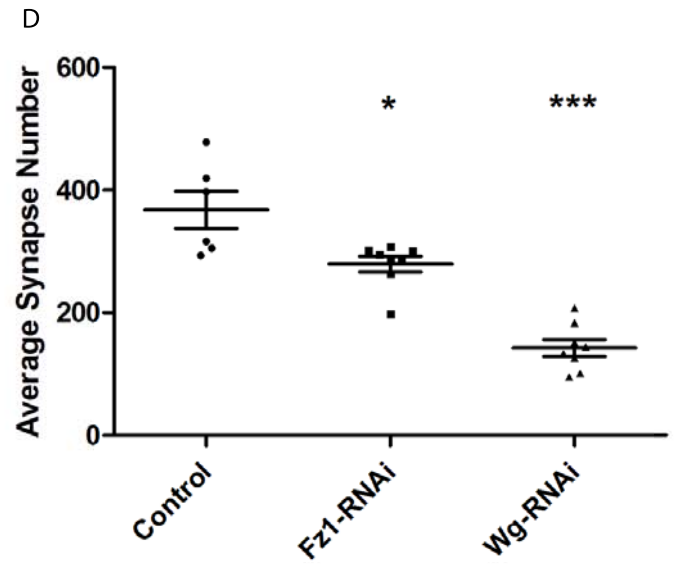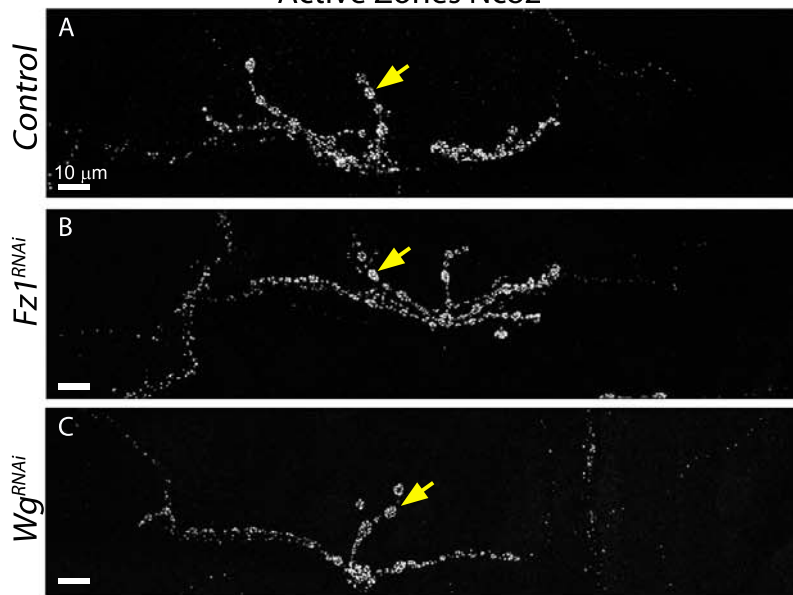1522
1523
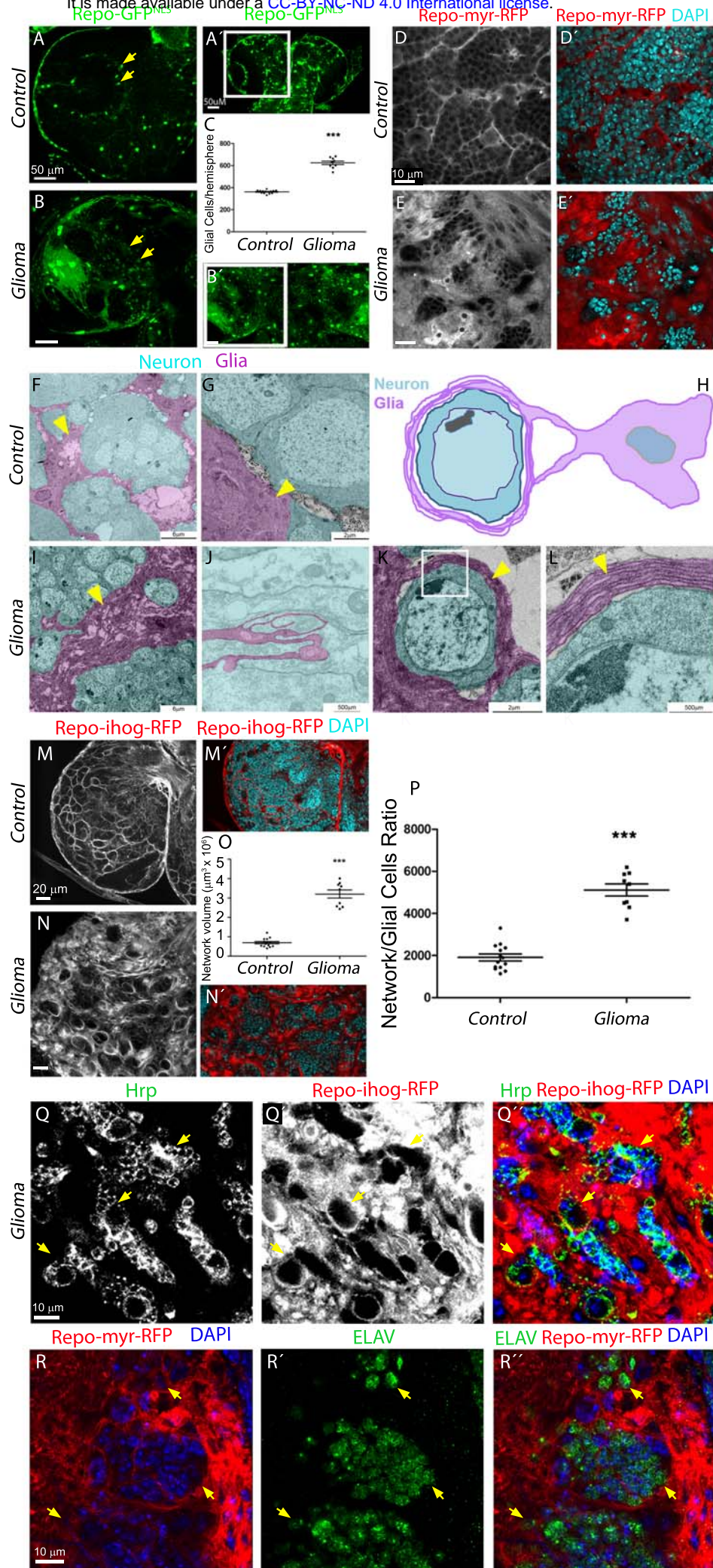
Portela Fig 1

Portela_Fig2

Portela_Fig3
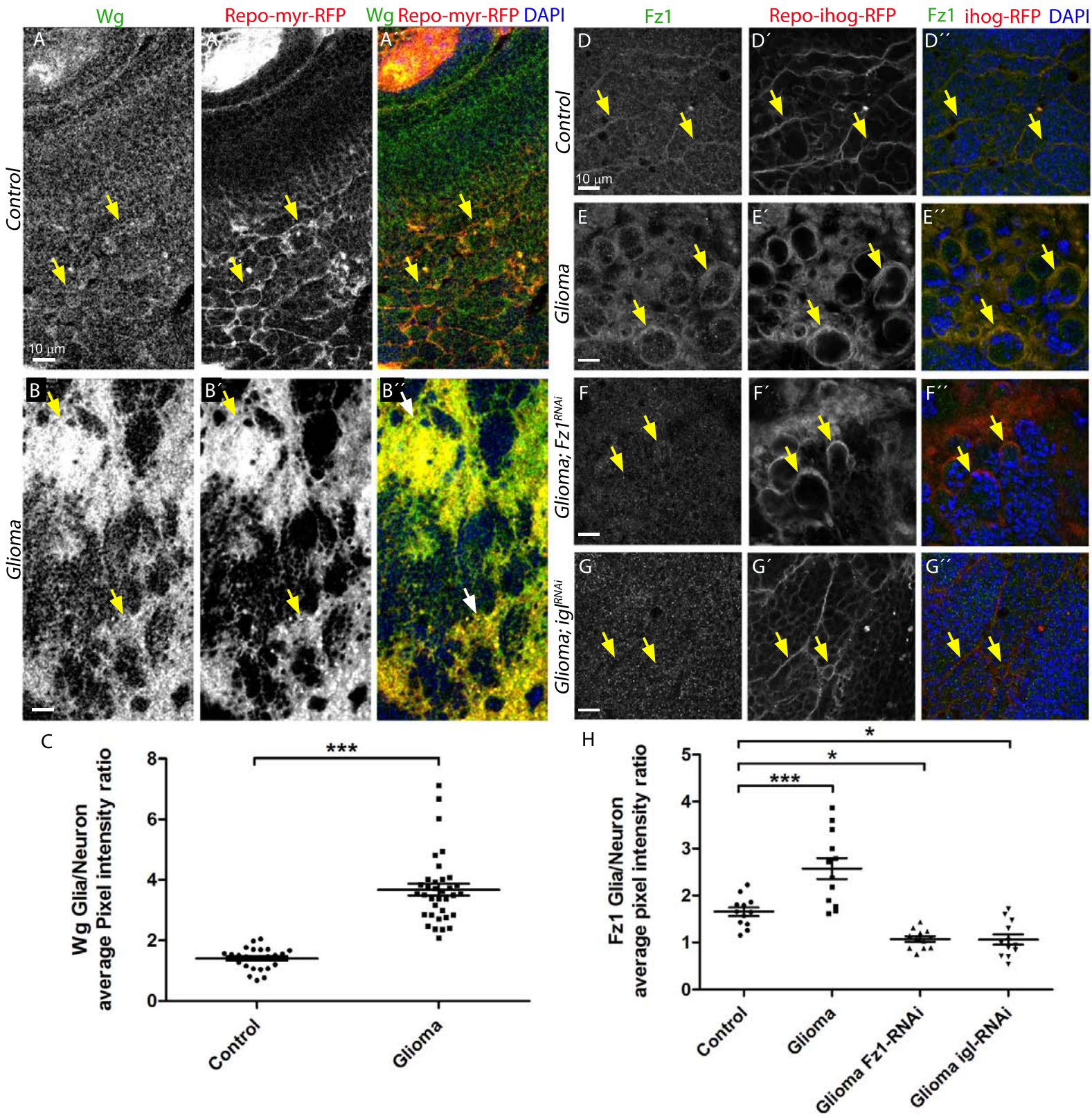
Portela_Fig4

Portela_Fig5

Portela_Fig6

Portela_Fig7

Portela_Fig8